A Combined Approach of Quantitative Interaction Proteomics and Live-cell Imaging Reveals a Regulatory Role for Endoplasmic Reticulum (ER) Reticulon Homology Proteins in Peroxisome Biogenesis*[S]

Christine David‡, Johannes Koch‡**, Silke Oeljeklaus§, Alexandra Laernsack‡, Sophie Melchior‡, Sebastian Wiese§, Andreas Schummer§, Ralf Erdmann¶, Bettina Warscheid§‖, and Cécile Brocard‡‖**

Peroxisome biogenesis initiates at the endoplasmic reticulum (ER) and maturation allows for the formation of metabolically active organelles. Yet, peroxisomes can also multiply by growth and division. Several proteins, called peroxins, are known to participate in these processes but little is known about their organization to orchestrate peroxisome proliferation. Here, we demonstrate that regulation of peroxisome proliferation relies on the integrity of the tubular ER network. Using a dual track SILAC-based quantitative interaction proteomics approach, we established a comprehensive network of stable as well as transient interactions of the peroxin Pex30p, an integral membrane protein. Through association with merely ER resident proteins, in particular with proteins containing a reticulon homology domain, and with other peroxins, Pex30p designates peroxisome contact sites at ER subdomains. We show that Pex30p traffics through the ER and segregates in punctae to which peroxisomes specifically append, and we ascertain its transient interaction with all subunits of the COPI coatomer complex suggesting the involvement of a vesicle-mediated transport. We establish that the membrane protein Pex30p facilitates the connection of peroxisomes to the ER. Taken together, our data indicate that Pex30p-containing protein complexes act as focal points from which peroxisomes can form and that the tubular ER architecture organized by the reticulon homology proteins Rtn1p, Rtn2p and Yop1p controls this process. ***Molecular & Cellular Proteomics 12: 10.1074/mcp.M112.017830, 2408–2425, 2013.***

From the ‡University of Vienna, Max F. Perutz Laboratories, Center of Molecular Biology, Department of Biochemistry and Cell Biology, Dr. Bohr-Gasse 9, A-1030, Vienna, Austria; §Faculty of Biology and BIOSS Centre for Biological Signalling Studies, University of Freiburg, 79104 Freiburg, Germany; ¶Institute for Physiological Chemistry, Department of Systems Biochemistry, Faculty of Medicine, Ruhr University of Bochum, 44780 Bochum, Germany

Received February 8, 2012, and in revised form, May 15, 2013
Published, MCP Papers in Press, May 20, 2013, DOI 10.1074/mcp.M112.017830

All nucleated cells contain essential round-shaped organelles called peroxisomes, whose function is mainly associated with lipid metabolism (1). Depending on the cellular requirements, the size, number, and protein content of these single membrane-bound organelles can vary widely. Although peroxisomes are dispensable for unicellular species such as yeasts, they are essential for the development of multicellular organisms (2, 3). In human, mutations in *PEX* genes lead to defects in peroxisome function or formation and are associated with the development of lethal pathologies (4). These *PEX* genes code for proteins, called peroxins, which are involved in peroxisome assembly and maintenance (5).

Two major routes seem to lead to peroxisome formation, namely, *de novo* biogenesis and growth/division of pre-existing peroxisomes. The division pathway operates with proteins of the Pex11 family and requires fission factors shared with mitochondria (6). Studies in yeast and mammalian cells revealed that through the action of the protein Pex3p peroxisome precursors can also originate from the endoplasmic reticulum (ER)[1] and, via import of membrane and matrix proteins, mature into fully functional organelles (7, 8). Furthermore, several peroxisomal membrane proteins were shown to migrate to peroxisomes via the ER (7, 9, 10). The molecular mechanism underlying the biogenic pathway of peroxisome formation has not been clarified so far. Recent data based on cell-free vesicle-budding reactions, however, demonstrated that several peroxisomal proteins traffic from the ER to peroxisomes in a COPII vesicle-independent manner (11). These observations point to the existence of vesicular events to

[1] The abbreviations used are: ER, endoplasmic reticulum; AP-AM, affinity-purification after mixing; AP-PM, affinity-purification prior to mixing; EPCONS, ER-to-peroxisome contact sites; GFP, green fluorescent protein; MS, mass spectrometry; PEX, peroxin; RFP, red fluorescent protein; RHPs, reticulon homology-domain proteins; SILAC, stable isotope labeling with amino acids in cell culture; TAP, tandem affinity-purification; TEV, tobacco etch virus.

mediate the transport of peroxisomal membrane proteins from the ER. In fact, analysis of secretory mutant yeast cells already suggest that part of the ER-associated secretory machinery is involved in peroxisome biogenesis (12).

The *de novo* biogenesis of peroxisomes and the growth/division pathways are usually seen as independent routes; however, these events may be coordinated and, thus, intimately linked. Indeed, peroxisomes need to acquire membrane components to proliferate and it has been proposed that their binding to the cell cortex or to the cytoskeleton allows their partitioning and segregation during cell division (13–15).

Among the proteins required for assembly of peroxisomes, the membrane proteins Pex23p and Pex24p play essential roles in the yeast *Yarrowia lipolytica* (16, 17). Homologs of these two proteins in *Saccharomyces cerevisiae* are Pex30p, Pex31p, and Pex32p, all containing at least one transmembrane domain and a dysferlin domain as common structural motifs, as well as Pex28p and Pex29p. In *S. cerevisiae*, these proteins seem to negatively control peroxisomal size and number (18, 19). Interestingly, Pex30p seems to exhibit species-specific differences in the regulation of peroxisome proliferation. While the lack of Pex30p in *S. cerevisiae* leads to an increase in the number of normal-sized peroxisomes (18), in *Pichia pastoris* its absence correlates with the appearance of fewer and clustered peroxisomes (20). Although peroxisomes are highly versatile organelles, under given conditions their total number per cell remains fairly constant owing to the delicate balance of proliferation, inheritance and degradation (21, 22). The question is: what are the molecular mechanisms responsible for the spatiotemporal organization of these events?

Here, we present data obtained from a dual approach based on quantitative interaction proteomics using stable isotope labeling with amino acids in cell culture (SILAC) (23, 24) and live-cell imaging, revealing for the first time the dynamic interaction network around Pex30p and its function in the organization of ER-to-peroxisome membrane associations. We report the existence of a macromolecular membrane protein complex that acts as a hub for the regulation of peroxisome proliferation and movement. Our data suggest a direct role for the tubular cortical ER and the reticulon homology proteins Rtn1p, Rtn2p, and Yop1p in the regulation of peroxisome biogenesis. Furthermore, as an initially cortical-ER localized protein that interacts with reticulon homology proteins, Pex30p is shown in this work to establish contacts between ER tubules and peroxisomes and to specifically traffic through the ER. In summary, our data reveal a central role for Pex30p in the formation of ER-to-peroxisomes associations that appear to be involved in the coordination of peroxisome biogenesis and maintenance.

EXPERIMENTAL PROCEDURES

Plasmids and Cloning Techniques—Plasmids were amplified in the *Escherichia coli* strain DH5α (25). *ADH1prom*-mCherry-Px (pCB741) was created by cloning the amplified *ADH1*-promoter (SacI/XbaI; primers: H911/H912) and mCherry-Px (XbaI/HindIII; primers CB293/CB112) into YEplac195. *MLS*prom-BFP-Px (pCB 579) was created by cloning the amplified BFP-Px (primers: CB180/CB181) via a pGEM-T vector (Promega, Madison, WI) into pJR233 conferring uracil prototrophy (BamHI/HindIII). To create the plasmid pBFP-Px (pCB 858), BFP-Px was shuttled into pCB633 (BamHI/HindIII) for leucine prototrophy. *GALSprom-PEX30-GFP* was created by PCR using genomic DNA as template (CB517, primers CB320/CB244), cloned into the pGEM-T vector to give rise to pCB822 and subcloned into a YEplac181 vector (SphI/PstI) resulting in pCB823. *GALSprom*-PEX30-mCherry (pCB855) was established by substituting DsRed by mCherry (BstXI/KpnI) from a PCR product (primer: CB406/407) in pCB854 previously obtained via cloning the amplified *GALSprom-PEX30*-DsRed from genomic DNA (CB509, primers: CB388/CB389) into a YEplac112 (SphI/KpnI). *GALSprom-PEX32-GFP* (pCB849) was obtained by replacing *PEX30-GFP* (pCB823; XbaI/PstI) with *PEX32-GFP* amplified from genomic DNA (CB214, primers: CB381/CB382). Similarly, for *GALSprom-PEX29-GFP* (pCB851), *PEX32-GFP* was replaced by *PEX29-GFP* (BglII/PstI) amplified from genomic DNA (CB208, primers: CB383/CB382). *PEX29* and its cognate promoter were amplified by PCR using genomic DNA as template (CB80A; primers: CB203/H869) and cloned into YEplac195 (SalI; pCB747). The *ADH1prom-PEX29* construct (pCB746) was created by cloning the PCR-generated *PEX29* (primers: CB301/H891) into the YEplac195-*ADH1*p construct (SalI/PstI) mentioned above. The plasmid containing *GPDprom-PEX*11 has been described previously (26). pCB861 containing *GPDprom-PEX25* was obtained from recombination of pENTR4-*PEX25* (27) with the destination vector pAG416-*GPD* (Euroscarf) using the GATEWAY technology (Invitrogen). The plasmids coding for Sec63p-RFP and Sec63p-GFP controlled by the *SEC63* promoter were a kind gift from Jeffrey Gerst (Rehovot, Isreal). Plasmid pCB842 was created from pFA6-natNT2 (Euroscarf) by inserting *ADH1prom*-mCherry-Px (SacI) obtained via PCR (pCB741, primers: CB348/CB349). To create pCB856, *ADH1prom-mCherry-Px* was cloned into pCB840 (SacI, (26)). For the integration into the *S. cerevisiae* genome, PCR fragments were generated using the templates pFA6-hphNT1 (Euroscarf), pCB842 (*ADH1prom-mCherry-Px::natNT2*), or pCB856 (*ADH1prom-mCherry-Px::hphNT1*) and the appropriate primer pairs as indicated in supplemental Table S1 and transformed using standard procedures. All genomic integrations were tested by PCR and Southern blot when required. Standard techniques were used for transformation, sporulation and tetrad analysis of yeasts. Standard procedures were used for DNA engineering and bacterial transformation.

Yeast Culture Conditions—The *S. cerevisiae* strains used are listed in supplemental Table S2. Cells were grown in SC medium (0.67% yeast nitrogen base) or in SC medium supplemented with 1% yeast extract and the appropriate amino acids as well as 2% D-glucose (Dextrose) or 2% galactose. Unless otherwise stated, cells were shifted to galactose medium for 15 min to induce *GAL*-driven *PEX30* expression followed by 15 min incubation in glucose medium. To induce peroxisome proliferation, cells were grown in YNO (0.67% yeast nitrogen base, 0.1% oleic acid, 0.05% Tween 80, pH 6.0 with KOH). For inheritance assays, cells were diluted to OD600 nm = 0.1 and 0.5 μl were plated onto agarose pads. For biogenesis assays, cells were cultured in glucose containing medium for 3 days prior to galactose induction. Oleic acid utilization assays were performed as described (28).

Western Blot Analysis—For Western blot analyses proteins were loaded onto a 10% SDS gel, separated by electrophoresis (BioRad) and transferred onto nitrocellulose (transfer buffer: 25 mM Tris, 500 mM glycin) using a semi-dry blotting apparatus [60 mA constant (1.5 mA/cm^2), 25 V max.] for 2 h. The membrane was then washed once

in TBST (50 mM Tris, 150 mM NaCl, 0.05% v/v Tween 20), incubated in blocking solution (TBST supplemented with 4% w/v low fat milk powder) for 1 h, subsequently briefly washed and incubated with the primary antibody for 2 h at room temperature. Following a washing procedure (3 times 15 min in TBST), incubation with the horseradish peroxidase conjugated secondary antibody was performed for 1.5–2 h. Detection was performed by chemoluminescence using the Super Signal West Pico Chemiluminescent Substrate (Pierce).

Antibodies—Rabbit-anti-Pex30p antibodies (1:30,000) were produced using an affinity-purified fraction of the N-terminal 164 amino acids of Pex30p expressed in *E. coli* BL21. Mouse-anti-porin antibodies (1:10,000) were purchased from Molecular Probes. Rabbit-anti-COPI coatomer antibodies (1:1,000) directed against the whole coatomer complex (Ret1p or α-COP1, 135.6 kDa; Sec26p or β-COP1, 109.0 kDa; Sec21p or γ-COP1, 104.8 kDa; Sec27p or β'-COP1, 99.4 kDa; Ret2p or δ-COP1, 60.6 kDa; Sec28p-ε-COP1, 33.8 kDa and Ret3p or ζ-COP1, 21.7 kDa) were a kind gift from Anne Spang (Basel, Switzerland) and described in Sandmann *et al.* (29). Rabbit-anti-Pex3p (1:5,000) and anti-Pex14p (1:5,000) antibodies were described before (30, 31). Rabbit-anti-Kar2p antibodies (1:20,000) were a kind gift from Ben Distel (University of Amsterdam, The Netherlands). HRP-conjugated sheep-anti-mouse and donkey-anti-rabbit antibodies (1:10,000) were purchased from GE Healthcare. Rabbit-anti-Protein A antibodies (1:10,000) were purchased from Sigma Aldrich.

Isolation Of Membrane Protein Complexes—For SILAC-based quantitative affinity-purification mass spectrometry (AP-MS) analyses, we used isogenic yeast strains auxotrophic for lysine and arginine (*i.e.* CB200 and CB392 for the purification of the Pex30p complexes, CB199 (32) and CB513 for the Pex29p complexes; see supplemental Table S2). Quantitative AP-MS experiments were performed essentially as described previously (32). Briefly, yeast cells were grown to OD600 nm = 1 in SC medium containing 0.3% glucose, 5 × YNO medium was then added to induce peroxisome proliferation for 16 h. Control yeast cells expressing native Pex30p and Pex29p (CB199 and CB200), respectively were grown in medium complemented with $^{13}C_6$-coded "heavy" lysine and arginine (50 mg/l each), whereas the cells from the corresponding TAP-tagged strains (CB392 and CB513) were grown in medium containing 50 mg/l $^{12}C_6$-coded "light" lysine and arginine. LC/MS analyses of protein extracts from lysine and arginine auxotrophic cells revealed that > 99% of all peptides showed complete incorporation of heavy lysine and arginine (supplemental Fig. S1).

In AP-AM experiments, differentially labeled cells were mixed at 1:1 ratio in net weight immediately after harvest. Affinity purification of native protein complexes using IgG-Sepharose was carried out as described previously (33) with some modifications. Yeast cells were lysed with glass beads in buffer containing 20 mM HEPES pH 7.5, 100 mM KOAc, 5 mM $Mg(OAc)_2$, 2 mM PMSF, 10 mM NaF and 10% glycerol, 0.3% digitonin, 2 μg/ml aprotinin, 0.35 μg/ml bestatin, 2.5 μg/ml leupeptin, 1 μg/ml pepstatin. The lysates were centrifuged at 100,000 × *g* and the resulting pellets (adjusted to 3.3 mg protein/ml) were solubilized using 1% digitonin. After centrifugation at 100,000 × *g* the solubilized extracts were subjected to affinity-purification using human IgG conjugated to a CNBr-activated-Sepharose matrix and crosslinked with DMP. For mass spectrometric analysis, proteins in TEV eluates were precipitated using ice-cold acetone and resuspended in 0.1 M NaOH/1% SDS. 2 × Laemmli sample buffer containing 8 M urea was added and proteins were separated on a 4–12% Bis-Tris NuPAGE gel (Invitrogen, Carlsberg, CA) according to the manufacturer's instructions.

In SILAC AP-PM experiments, isolation of membrane protein complexes was carried out separately for each strain. The TEV eluates originating from control and TAP-tagged strains were equally mixed before acetone precipitation and proteins were separated by SDS-PAGE as described above.

For co-immunoprecipitations using TAP-tagged Pex30p, Rtn1p, and COPI components or Protein A-tagged Pex14p as bait, cells were lysed with glass beads in lysis buffer supplemented with 1 mM EDTA. Crude extracts (5 mg protein/ml) were directly solubilized with 1% digitonin for 30 min at 4°C and centrifuged at 100,000 × *g* before incubation with human IgG-Sepharose matrix and further processed as described above with the exception that after washing, the IgG-Sepharose was split into two equal parts. In one part the bound proteins were eluted via TEV protease digestion, in the other part proteins attached to the matrix were eluted using SDS-sample buffer as indicated in Fig. 3.

LC/MS Analysis—Following separation of affinity-purified proteins by SDS-PAGE and staining with colloidal Coomassie Blue G-250, gel lanes were cut into 20 slices and processed for mass spectrometric analysis of tryptic peptide mixtures as described previously with slight modifications (34). Briefly, nano HPLC/ESI-MS/MS analyses were performed using the UltiMate™ 3000 HPLC system (Dionex LC Packings, Idstein, Germany) directly coupled to an LTQ-Orbitrap XL instrument (Thermo Fisher Scientific, Bremen, Germany). The HPLC system was equipped with two C18 μ-precolumns (0.3 mm inner diameter × 5 mm, particle size 5 μm; PepMap, Dionex LC Packings) and a C18 RP nano LC column (75 μm inner diameter × 150 mm; particle size 5 μm; PepMap, Dionex LC Packings). Peptides were eluted using a 30-min linear gradient ranging from 4 to 40% (v/v) acetonitrile in 0.1% (v/v) formic acid. The LTQ-Orbitrap XL, equipped with a nanoelectrospray ion source (Thermo Fisher Scientific) and distal coated SilicaTips, was externally calibrated using standard compounds and lock masses were used for internal calibration. The instrument was operated using the following parameters: spray voltage, 1.6 kV; capillary voltage, 45 V; capillary temperature, 200°C; tube lens voltage, 100 V. Full scan MS spectra (*m/z* 300–1500; resolution of 30,000 at *m/z* 400) were acquired in the orbitrap. After a brief survey scan, the four most intense multiply charged ions were selected for fragmentation by low energy collision-induced dissociation in the linear ion trap simultaneously with the completion of the MS scan in the orbitrap. Automatic gain control for the orbitrap and the LTQ were set to 5×10^5 and 10,000 ions, respectively, with a maximum fill time of 750 ms (orbitrap) and 150 ms (LTQ). Fragmentation was performed at a normalized collision energy of 35% with an activation $q = 0.25$ and an activation time of 30 ms. The ion selection threshold was set to 500 and a dynamic exclusion time for fragmentation of previously selected precursor ions of 60 s was applied.

Mass Spectrometric Data Analysis and Statistics—For protein identification and SILAC-based relative protein quantification, mass spectrometric raw data were processed using MaxQuant [version 1.0.13.13 (35)]. Peak lists of MS/MS spectra generated by MaxQuant were filtered to contain at most six peaks per 100 kDa interval and searched against a decoy version of the *Saccharomyces* Genome Database (SGD; http://www.yeastgenome.org; version of June 6, 2008) containing 13,434 entries that included the original and a shuffled variant of each protein sequence. The decoy database was generated using the publically available Decoy Database Builder as described (36). Species restriction to *S. cerevisiae* is justified because exclusively proteins from baker's yeast were analyzed in this work. Database searches using Mascot [version 2.2, Matrix Science (37)] were performed with the following parameters: mass tolerances for parent and fragment ions, 7 ppm and 0.5 Da, respectively; tryptic specificity allowing two missed cleavages and three labeled amino acids; variable modifications, oxidation of methionine; fixed modifications, none. $^{13}C_6$-arginine and -lysine were set as heavy labels and a false discovery rate of 0.01, calculated as described earlier (35), was applied for both peptides and proteins. Proteins were identified based

on at least one unique peptide with a minimum length of six amino acids. If proteins were not distinguishable based on the set of peptides identified, they were combined by MaxQuant and listed as protein group. Only proteins identified in at least two out of three replicates and/or with a total of at least two unique peptides are reported in this work (supplemental Tables S3*A*, S4*A*, and S5*A*).

Relative protein quantification by MaxQuant is based on two-dimensional centroid intensities of peptide pairs (see ref. 35 for more details) and was performed using the following parameters: only unique peptides were quantified; minimum ratio count, one; "Re-quantify" was enabled; "Filter labeled amino acids" and "Keep low-scoring versions of identified peptides" were disabled. Protein ratios determined by MaxQuant are the median of all peptide ratios of a distinct protein or protein group. The corresponding variability (in %) is the standard deviation of the ln-transformed peptide ratios used to calculate the protein ratio multiplied by 100 (38).

To discriminate between specific interaction partners and contaminants in AP-AM and AP-PM experiments ($n = 3$ each), proteins with abundance ratios differing significantly and consistently from 1 were detected using the *t* test method. In this work, a one-sided *t* test was used as proteins were tested for enrichment applying a significance level of 5% (alpha-value). To further assess the power of AP-MS experiments with sample sizes of $n = 2$ and $n = 3$ per group, a power analysis was performed based on a representative standard deviation (S.D.) using the pwr-package for the R environment (http://cran.r-project.org/web/packages/pwr/index.html). Since the 90%-quantile of the SDs observed in all individual proteins was used, only 10% of SDs were higher than the selected value. Ratio thresholds with a common power of 80% for sample sizes of $n = 2$ and $n = 3$ were calculated for each AP-MS experiment. Proteins with p values < 0.05 and significant abundance ratios as determined by power analysis for each dataset were considered true components of Pex29p and Pex30p complexes.

Protein and peptide identification and quantification results as well as data derived from statistical data analyses are provided as supplemental material (Tables S3*A*–S3*C*, S4*A*–S4*C*, and S5*A*–S5*C*). Mass spectrometric raw data, Mascot search results (dat files), and MaxQuant result files of all experiments are stored at the scientific file sharing network and data repository Tranche and may be downloaded from https://proteomecommons.org/tranche/using the following hash: YvRoNkiCWfqxGystvV9cds3i/e1GdAHyS2ZKRn/yxxc53sd1mYi4CrFZjjMaft7 VUEMivBY/dW49vLcG+V9zFM5h1GcAAAAAAADKaQ==.

Microscopy and Live-cell Imaging—After galactose induction, cells were cultured in YNO for 8 h and subsequently transferred onto agarose pads precast on objective slides and imaged immediately. For live-cell imaging, the pad medium was identical to the growth medium supplemented with 1.7% low-melting agarose. Microscopy was performed on an Olympus CellR work station (Objective: UPLSAPO 60 × 1.42; Camera: Hamamatsu Orca ER; Filter sets: BFP exc: 330–385 nm, em: LP420 nm; GFP exc: 457–487 nm; em: 503–538 nm; mCherry exc: 579–596 nm, em: 618–664 nm; Pixel spacing 107 × 107 × 300 nm or 107 × 107 × 1000 nm for live-cell imaging).

FRAP Experiments—For FRAP experiments, cells were treated as described above except for induction of *GAL*-expression for 2 h before microscopic analysis. Cells were immediately transferred onto agarose pads and imaged on an LSM 510 META unit (Objective α-NeoFluar 100 × 1.45; Filter set: MBS488, LP505; Laser: 488 nm; Pixel spacing: 30 × 30 nm; Pixel dwell time: 2.7 μs). Bleaching was performed after three prescans on multiple small areas of 0.5 μm^2 and recovery was monitored until saturation.

Trajectory Analysis—Cells lacking Pex30p and cells expressing Pex30p-GFP were imaged live as described above, but in 1 min intervals for 0.5 h. After deconvolution, the tracks were extracted and analyzed using the SPT software package as described previously (39). Briefly, the trajectory analysis consists of two parts, 1) particle recognition and trajectory creation, and 2) trajectory analysis. The parameters used for particle recognition were the same for all images and tracks longer than 20 (of 30) frames were used for analysis. The trajectories of all mCherry-Px dots (peroxisomes) from more than 10 different cells were analyzed for each strain. The analysis is based on the calculation of the moments of displacements μ_ν (39) and plotting log μ_ν *versus* the total time interval. Plots were created for the first 10 moments of displacement $\mu_\nu(\nu = 1, 2, \ldots, 10)$ and the respective scaling coefficient γ_ν was extracted through a linear least squares fit. To calculate the mean square displacement (MSD), the second order of displacement ($\nu = 2$) was used to calculate the two-dimensional diffusion coefficient D_2 (y-intercepts). For strong self-similar movements, D_2 represents the regular diffusion coefficient. The moment scaling spectrum (MSS) was produced by plotting the first 10 scaling coefficients in function of the order of the respective moment. In the analyzed scenario, most trajectories were strongly self-similar as confirmed by the linearity of the MSS curve. Here, the slope gives appraise for the type of motion: slopes < 0.5 correspond to subdiffusive, slopes > 0.5 to superdiffusive and slopes around 1 to ballistic movements. Values for the generalized two-dimensional diffusion coefficients D_2 and for the MSS-slopes (S_{MSS}) were exported from the SPT software and a scatter plot was arranged with a two-dimensional box plot. Each box ranging from the first to the third quartile contains 50% of the data points. The whiskers encompass 95% of the data, excluding the topmost and bottommost 2.5%. To estimate the statistical difference between the data sets, a Wilcoxon rank sum test was performed on https://elegans.swmed.edu/~leon/stats/*U* test.html.

Image Processing, Analysis and Counting of Peroxisomes—All images except for those shown in Fig. 4*D* were deconvolved as 3D data sets with an experimentally derived PSF using the CMLE algorithm in Huygens Professional (SVI, The Netherlands). Blue or white cell surroundings were obtained from transmission images through blurring and artificial colorizing. For statistical analysis of the total number of peroxisomes per cell, fluorescent spots (mCherry-Px) were counted manually on 3D data sets of more than 100 single cells and at least three independent cultures for each strain. Colocalization analyses were performed using the ImageJ Plugin "Colocalization Colormap" based on the normalized mean deviation product (nMDP) described previously (40). A colorized heat-map provides spatial information about colocalizing pixels. Only cells expressing both proteins were considered for analysis and extracellular regions were excluded. For FRAP analyses, image intensities were quantified in ImageJ (NIH). Background was subtracted and the bleached signal was normalized to nonbleached areas. Signal intensity at time point 0 was set to 100%. Recovery was fitted using the function $y = a[1 - \exp(-bx)]+c$.

RESULTS

Evidence for the Role of Pex30p in the Regulation of Peroxisome Biogenesis—Proteins of the Pex11 family were previously shown to influence the number of peroxisomes and participate in the regulation of peroxisome proliferation (41, 42). To test whether Pex30p acts in concert with these factors to maintain the steady state level of peroxisomes, we evaluated the total number of peroxisomes per cell in different yeast mutants incubated in oleic acid-containing medium (Fig. 1*A*). Cells lacking Pex30p exhibited more peroxisomes than wild-type cells (8.8 ± 1.5 *versus* 7.7 ± 1.4; n > 100). When Pex30p was expressed in *pex30*Δ cells the number of peroxisomes decreased virtually to wild-type levels (Fig. 1*A*). Inter-

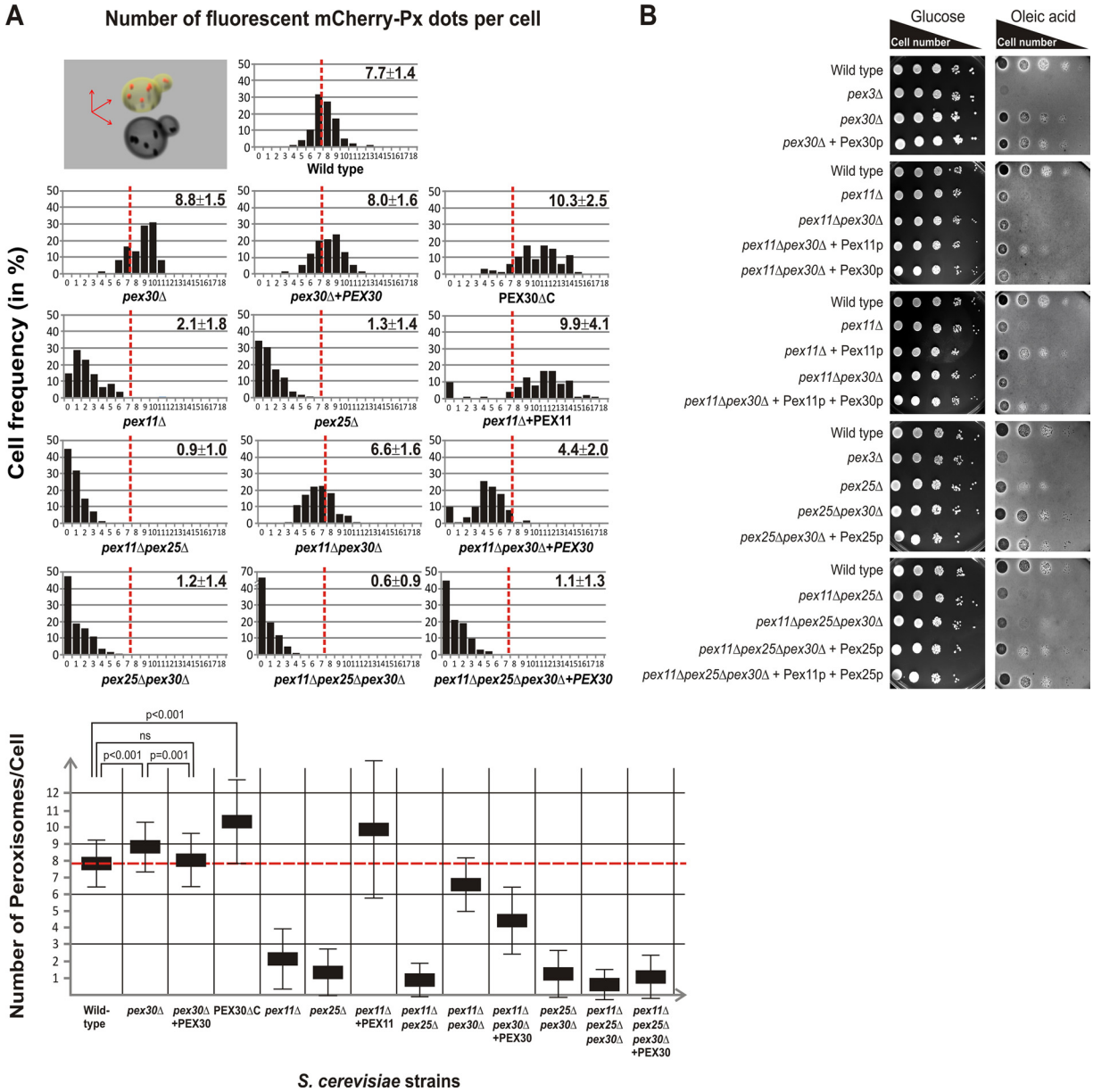

FIG. 1. **Pex30p and Pex11p act at different steps of peroxisome proliferation**. *A*, Quantitative distribution of peroxisomes in yeast cells with various genetic backgrounds (as indicated) expressing mCherry-Px (red channel) as illustrated in a 3D model. Yeast cells were transformed with plasmids expressing *PEX30* driven by the *GAL* promoter or *GPD*-controlled *PEX11* or *PEX25*. The mutant cells *PEX30ΔC* expressed a truncated version of Pex30p lacking amino acids 375–523 from the *PEX30* genomic locus. After galactose induction, cells were further incubated in medium containing oleic acid to induce peroxisome proliferation and observed 8 h later. For each yeast strain, fluorescent dots (mCherry-Px) were counted in three dimensions through a whole Z-stack in at least 100 cells from three independent cultures. The histograms illustrate the frequency distributions of cells (in percent) with a distinct number of peroxisomes. The average number of fluorescent mCherry-Px dots per cell is indicated as mean ± S.D. and tested for statistical significance (bottom panel). The dashed red lines represent the average number of peroxisomes in wild-type cells. *B*, Yeast cells with various genetic backgrounds, as indicated untransformed or transformed with plasmids expressing Pex11p, Pex25p, Pex30p or combinations, were grown to logarithmic phase in glucose medium and 10-fold serial dilutions were spotted onto solid medium containing either glucose or oleic acid. The function of peroxisomes was monitored through visualization of oleate use which led to the occurrence of transparency in the solid medium.

estingly, upon deletion of the last 229 amino acids (PEX30ΔC), ~50% of the cells contained more than 10 peroxisomes (10.3 ± 2.5; n > 100) showing that full length Pex30p was required to control peroxisome proliferation.

Huber *et al.* (26) have recently demonstrated that in *S. cerevisiae* the two members of the Pex11 family, Pex11p and Pex25p act differently on peroxisome proliferation. Although Pex11p was only required for the proliferation of pre-existing

peroxisomes, the presence of Pex25p was indispensable for *de novo* regeneration of peroxisomes from the ER (26). Thus, we examined the effect of deleting *PEX30* on cells lacking Pex11p or Pex25p. We consistently found few peroxisomes in *pex11*Δ (2.1 ± 1.8; $n > 100$), *pex25*Δ (1.3 ± 1.4; $n > 100$) and *pex11*Δ*pex25*Δ (0.9 ± 1.0; $n > 100$) mutant cells whereas overexpression of Pex11p (9.9 ± 4.1; $n > 100$) led to higher number of peroxisomes (Fig. 1*A*). Strikingly, when *PEX30* was deleted in *pex11*Δ mutant cells (6.6 ± 1.6; $n > 100$), the number of peroxisomes rose near wild-type levels demonstrating the potential of peroxisomes to proliferate in the absence of Pex11p. In contrast, deletion of *PEX30* in *pex25*Δ mutant cells did not lead to an increase in peroxisome number (1.2 ± 1.4; $n > 100$) and, in the absence of all three proteins, cells hardly contained peroxisomes (0.6 ± 0.9; $n > 100$). Overexpression of Pex30p in cells lacking Pex11p, Pex25p and Pex30p did not lead to a significant increase in the number of peroxisome per cell (1.1 ± 1.3; $n > 100$). Our data demonstrate that the function of Pex30p is required downstream of Pex25p, suggesting that Pex30p might rather be involved in the regulation of *de novo* formation of peroxisomes (see Fig. 1*A*; lower panel).

We analyzed whether variations in the number of peroxisomes per cell correlated with peroxisomal function in several mutant yeasts. In contrast to wild-type cells, *pex3*Δ mutant cells lack peroxisomes and, thus, are unable to perform β-oxidation and cannot use oleate as sole carbon source (Fig. 1*B*). The ability to consume the fatty acid was reduced in cells lacking Pex30p (Fig. 1*B*). Cells lacking *PEX11* displayed a severe growth defect on medium containing oleate. When Pex11p was expressed from a plasmid, these cells regained the ability to grow on this carbon source (Fig. 1*B*). In contrast to *pex11*Δ*pex30*Δ mutant cells, cells deleted for *PEX25* and *PEX30* could grow on oleate-containing medium. In agreement with the idea that Pex11p and Pex25p act in independent routes during peroxisome proliferation, peroxisomes were partially functional in *pex25*Δ cells, whereas they were nonfunctional in *pex11*Δ*pex25*Δ or *pex11*Δ*pex25*Δ*pex30*Δ mutant cells. Expression of Pex25p only, led to recovery of peroxisomal function in these cells (Fig. 1*B*). Furthermore, in favor of the notion that Pex30p and Pex25p act on the same pathway, mutant cells lacking both Pex25p and Pex30p could use oleate better than cells lacking only Pex25p.

Pex30p Interacts With ER-resident Proteins—To accurately identify Pex30p membrane protein interactions in *S. cerevisiae*, we employed SILAC-based AP-MS, a strategy that allows for unbiased and comprehensive analysis of protein complexes and large interaction networks (32, 43–45). To this end, isogenic yeast cells auxotrophic for lysine and arginine (*arg4*Δ*lys1*Δ) were differentially labeled via SILAC, grown under peroxisome-proliferating conditions and mixed in equal ratio. Note that these cells are indistinguishable from wild-type cells. They consume fatty acid added to the culture medium as sole carbon source and contain a similar number of peroxisomes (see supplemental Fig. S2*A* and S2*B*). Pex30p complexes were purified from digitonin-solubilized crude membrane fractions following a one-step purification protocol (affinity-purification after mixing, AP-AM; cartoon Fig. 2*A*). This method allows for the identification of native membrane protein complexes. Quantitative analysis of the mass spectrometric data obtained from three independent experiments by MaxQuant (35) was followed by statistical data evaluation and resulted in the classification of 20 proteins as specific constituents of the Pex30p membrane protein complex (Fig. 2*A*, 2D-plot, and supplemental Table S3). Among these were the bait Pex30p and Pex28p, Pex29p, and Pex32p, known factors in peroxisome proliferation (18, 19), as well as Rtn1p, Rtn2p, Yop1p, Pom33p, Spf1p, Scs2p, Ncp1p, Hfd1p, Dpm1p, Pho88p, Vac8p, Gsf2p, Sop4p, Pga3p, Emc4p, and Yet1p, all ER-membrane proteins involved in ER maintenance and function. Among all specific binding partners, our quantitative MS data point to the reticulon homology domain-containing proteins (RHPs) Rtn1p, Rtn2p, and Yop1p as the most abundant ER factors in the Pex30p complexes (Fig. 2*A*, 2D-plot, and supplemental Table S3*A*). The RHPs have been shown to maintain tubular ER structures through stabilization of high membrane curvature both in yeast and mammalian cells (46). These ER tubules represent connections between perinuclear and cortical ER domains as previously shown through microscopic analyses of the ER structure in the yeast *S. cerevisiae* (47).

Identification of Transient Interaction Partners of the Membrane Proteins Pex30p and Pex29p—Our initial AP-AM strategy applied to Pex30p complexes accurately identified stable interaction partners and, thus, allowed for the definition of the core components of the Pex30p interactome. However, in the AP-AM approach, identification of transient interaction partners exhibiting high on- or off-rates is biased because of exchange of components during affinity-purification (32, 43, 48, 49). To adequately tackle this issue, we performed separate affinity-purification experiments from SILAC-labeled cells expressing either wild-type (heavy) or TAP-tagged (light) Pex30p before combining affinity-purified samples for quantitative MS analysis (AP-PM; cartoon Fig. 2*B*). Application of the AP-PM strategy holds the potential to identify proteins with essential roles in modulating Pex30p function or localization that only transiently associate with the core complex. As a result of triplicate experiments, 36 proteins were classified as Pex30p interaction partners including numerous proteins previously identified in the AP-AM experiments. Among these were Pex28p, Pex29p, and Pex32p as well as the RHPs (Fig. 2*B*, 2D-plot, and supplemental Table S4*A*). We also identified the GTPase Sey1p, a functional ortholog of atlastins known to cooperate with Rtn1p and Yop1p to maintain the ER morphology (50). Interestingly, we observed that the entire COPI coatomer complex transiently associated with Pex30p complexes. The specificity as well as the transient nature of this association are reflected by the absence or very low

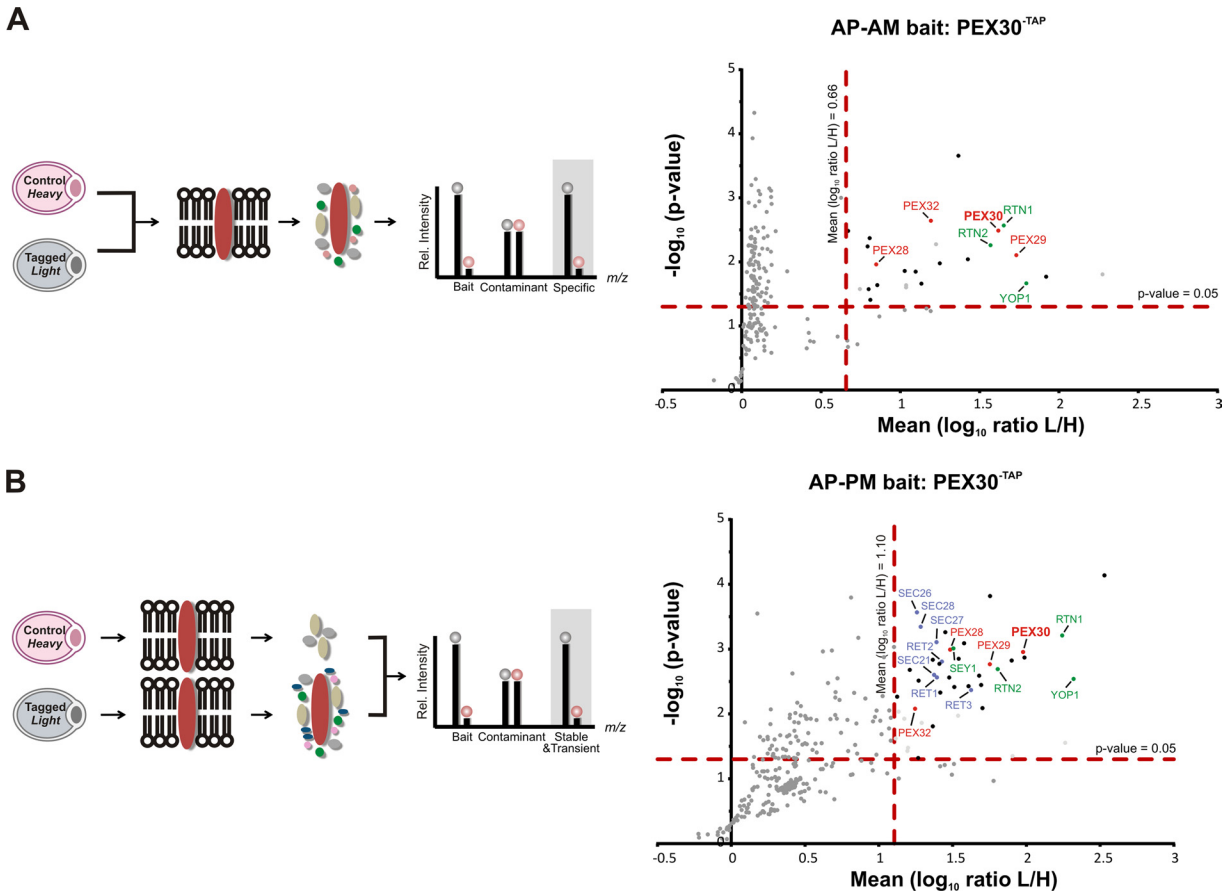

FIG. 2. **Dual-track SILAC-AP-MS analysis of Pex30p-containing membrane protein complexes.** Isogenic yeast cells auxotrophic for arginine and lysine and expressing either native (control, heavy) or TAP-tagged (tagged, light) Pex30p were grown under peroxisome-proliferating conditions and labeled using SILAC. *A*, Affinity-purification after mixing (AP-AM). After harvest, SILAC labeled cells were mixed in equal ratio and Pex30p complexes were affinity-purified from solubilized membrane fractions followed by quantitative MS analysis. Specific binding partners consistently showed high SILAC ratios, whereas proteins with ratios of approximately one were considered copurified contaminants. Proteins were plotted according to their *p* values ($-\log_{10}$) against the mean $\log_{10}$ SILAC ratios determined in three independent repeats. Specific binding partners illustrated in black and colored dots exhibit *p* values of ≤ 0.05 and mean $\log_{10}$ ratios "light-to-heavy" of ≥ 0.66 when quantified in 3/3 replicates and ≥ 1.66 in 2/3 replicates. The core components of Pex30p complexes are indicated. *B*, Affinity-purification prior to mixing (AP-PM). SILAC AP-PM experiments were performed to allow for identification of stable and transient interaction partners by quantitative MS. In addition to the bait and core components, specific transient binding partners also exhibited high SILAC ratios, whereas copurified contaminant showed ratios of approximately one. To define the interactomes of Pex30p, proteins were plotted according to their *p* values ($-\log_{10}$) *versus* the mean $\log_{10}$ SILAC ratios determined in triplicate experiments. Specific binding partners of Pex30p exhibit *p* values of ≤ 0.05 and mean $\log_{10}$ ratios "light-to-heavy" of ≥ 1.10 when quantified in 3/3 replicates and ≥ 2.79 in 2/3 replicates. Specific components of Pex30p complexes are labeled in black; red indicates peroxins involved in peroxisome proliferation, green ER proteins, blue subunits of the COPI coatomer complex.

abundance of COPI peptides derived from wild-type yeasts in AP-PM experiments (Fig. 3*A*), whereas COPI peptides showed a SILAC ratio of 1 in AP-AM experiments (supplemental Fig. S3*A*). In contrast, copurified contaminants such as Kgd1p are classified through a ratio of 1 and stable interaction partners through a consistently high SILAC ratio in both experimental setups (Fig. 3*A*, supplemental Figs. S3*A* and S3*B*). For further validation, we performed reverse affinity-purification experiments using cells expressing TAP-tagged copies of COPI coatomer subunits and tested for the presence of Pex30p in the eluates (Fig. 3*B*). In all cases, the intensity of the detected Pex30p signal correlated well with the amounts of coatomer complex purified, whereas no signal was detected in the purified importomer complexes using Pex14p as bait. Western blot analyses of the affinity-purified complexes of selected COPI subunits (Sec28p and Ret1p), Pex30p, and Pex14p further revealed that COPI subunits were present in Pex30p complexes whereas Pex14p neither copurified with Ret1p and Sec28p nor with Pex30p (supplemental Fig. S4). Our data thus demonstrate that Pex30p specifically associates with the coatomer complex.

Pex30p and Pex29p are believed to play a role in the same process and Pex29p has been proposed to act upstream of Pex30p in the regulation of peroxisome proliferation (18) sug-

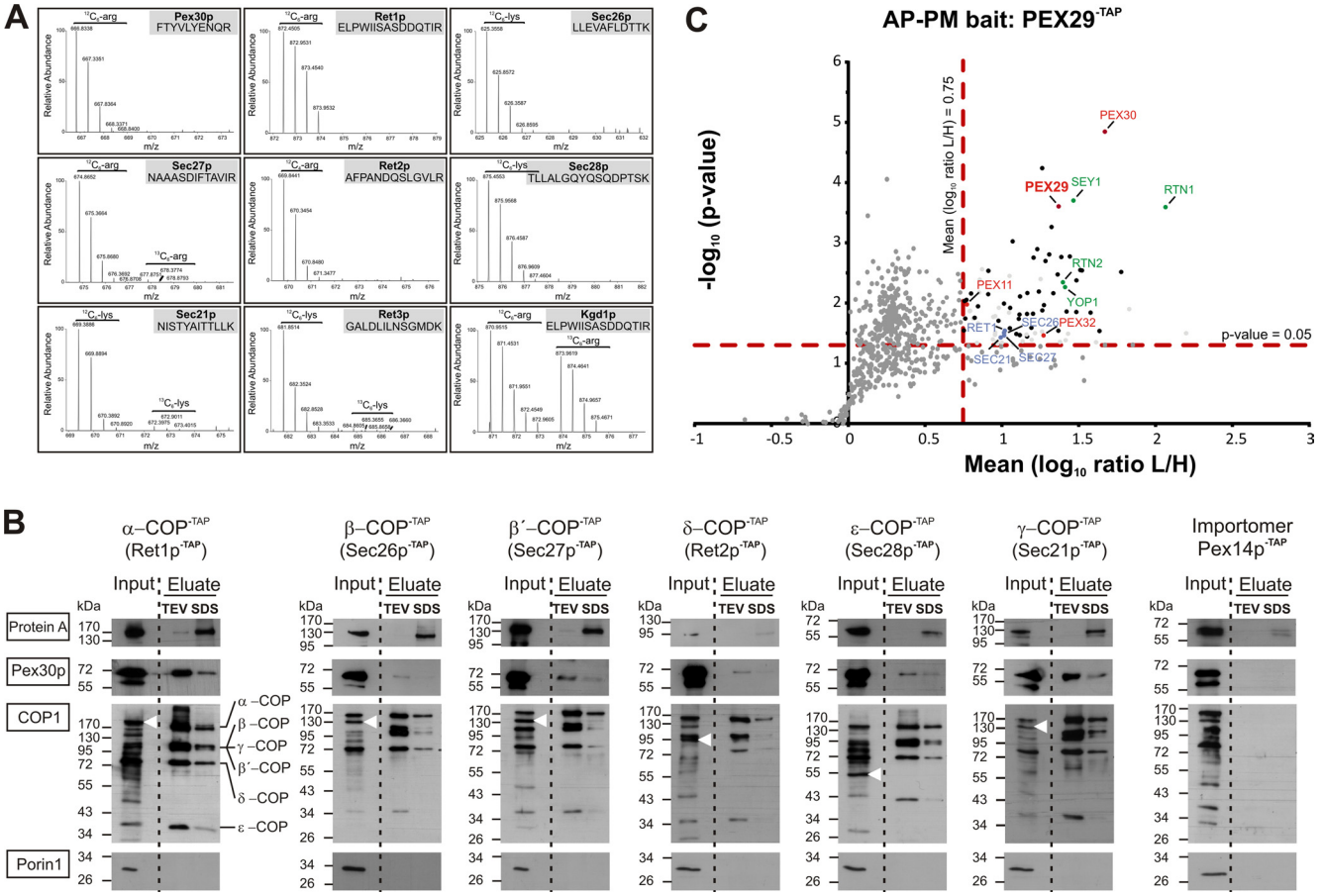

FIG. 3. **Pex30p specifically associates with the COPI coatomer complex.** *A*, Specific association between COPI components and Pex30p are exemplified by zoom-in MS survey spectra of SILAC-encoded peptides. *B*, Affinity purification of COPI components. Cells expressing TAP-tagged subunits of the coatomer complex or Pex14p-^{TAP}, a subunit of the peroxisomal importomer, were used for affinity purifications using IgG-coupled Sepharose beads. After washing, the Sepharose was split into two equal parts and proteins bound to the matrix were eluted via TEV protease digestion (TEV) or using SDS sample buffer (SDS). Whole cell lysates (Input) and the respective eluates were analyzed by immunoblotting with anti-Protein A, anti-Pex30p, anti-COPI or anti-Porin antibodies. Signals for the TAP-tagged COPI subunits show slower electrophoretic mobility in the input lanes because of the Protein A repeats (white arrowheads) but not in the TEV eluates. *C*, SILAC-based AP-PM experiments for Pex29p-containing membrane protein complexes. Isogenic yeast cells auxotrophic for lysine and arginine were used and three independent repeats were performed. Proteins are plotted by their *p* values (-$\log_{10}$) against the mean $\log_{10}$ SILAC ratios determined in AP-PM experiments ($n = 3$). Specific binding partners of Pex29p exhibit *p* values of ≤ 0.05 and mean $\log_{10}$ ratios "light-to-heavy" ≥ 0.75 and ≥ 1.89 when quantified in 3/3 and 2/3 replicates, respectively. Reticulon homology proteins and Sey1p are indicated in green. Four subunits of the COPI vesicle coatomer were found to transiently associate with Pex29p (indicated in blue).

gesting that these proteins might assemble in a protein complex. We addressed this issue in reverse SILAC AP-PM experiments ($n = 3$) using Pex29p as bait and identified a subset of the proteins present in Pex30p complexes such as Pex30p, Pex32p, Rtn1p, Rtn2p, Yop1p, and Sey1p as well as Ret1p, Sec21p, Sec26p, Sec27p, four components of the COPI coatomer (Fig. 3*C* and supplemental Table S5*A*). Note that although not classified as specific in the Pex30p complexes, Pex11p was found as specific binding partner in Pex29p complexes.

To conclude, through unbiased SILAC-based quantitative AP-MS analyses, we identified a large macromolecular complex around the integral membrane protein Pex30p; Pex28p, Pex29p, and Pex32p as well as Rtn1p, Rtn2p, and Yop1p are central core components, whereas the GTPase Sey1p and all subunits of the coatomer complex are transiently associated suggesting modular functions of Pex30p.

Pex30p Interacts with Rtn1p and Localizes to the Cortical ER—To evaluate whether the interaction of Pex30p with Rtn1p relied on the presence of the other peroxisomal proliferation factors, we performed affinity-purification of Rtn1p-TAP from different yeast mutants. Pex30p specifically copurified with Rtn1p-TAP (Fig. 4*A*). However, in the absence of Pex29p, higher levels of Pex30p coprecipitated with Rtn1p suggesting a competition between Pex29p and Rtn1p for Pex30p binding. To test this hypothesis, we compared the amounts of Pex30p copurifying with Rtn1p in different mutant backgrounds. In cells lacking Rtn2p, known to interact with Rtn1p,

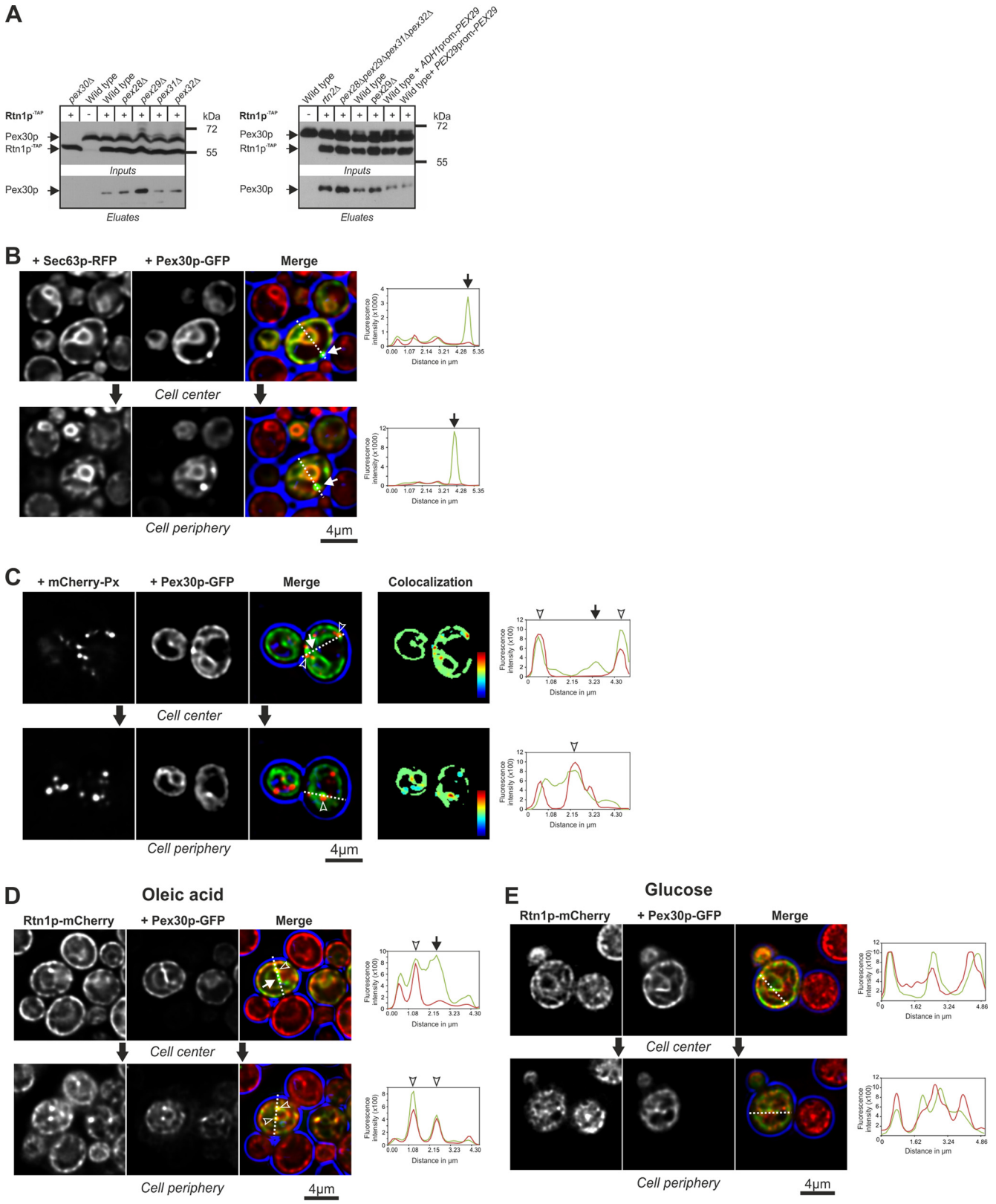

FIG. 4. **Pex30p accumulates at subdomains of the cortical ER in patches that coincide with Rtn1p.** *A*, Varying Pex29p levels affect the interaction between Rtn1p and Pex30p. Yeast cells with various genetic backgrounds (as indicated) expressing TAP-tagged Rtn1p (Rtn1p^{-TAP}) from their genomic locus were used for affinity-purification. Equal amounts of proteins from digitonin-solubilized membranes (Inputs) and

higher amounts of Pex30p copurified with Rtn1p and similarly in *pex29*Δ or *pex28*Δ*pex29*Δ*pex31*Δ*pex32*Δ mutant cells. Concurring, in cells expressing elevated levels of Pex29p, smaller amounts of Pex30p co-purified with Rtn1p (Fig. 4*A*). These data further illustrate that Pex30p and Rtn1p are likely involved in several interactions.

The results of our proteomic interaction analyses prompted us to assess the localization of Pex30p in yeast cells co-expressing Sec63p-RFP, a subunit of the ER translocon complex, and Pex30p-GFP in *pex30*Δ cells. To tune the *PEX30* expression levels, we transformed *pex30*Δ mutant cells with a plasmid expressing Pex30p-GFP controlled by the *GAL*-promoter. Our Western blot analysis of Pex30p-GFP levels established that induction through a 15 min galactose pulse followed by incubation of the cells in medium containing oleic acid was adequate to produce a signal for Pex30p-GFP comparable to wild-type levels (supplemental Fig. S2*C*). As illustrated in Fig. 4*B*, Pex30p-GFP partially colocalized with Sec63p-RFP, in particular at the nuclear periphery. In contrast, the fluorescent signals were higher for Pex30p-GFP than for Sec63p-RFP at the cortical ER and Pex30p-GFP structures were observed at the cell periphery that lacked Sec63p-GFP signal.

Next, we examined whether the observed Pex30p-GFP punctae represented peroxisomes and coexpressed the peroxisomal marker mCherry-Px and Pex30p-GFP. Interestingly, most mCherry-Px signal accumulated close to or coincided with Pex30p-GFP punctae as illustrated by the overlapping colors in the colocalization map (Fig. 4*C*). These observations suggest either that a portion of Pex30p trafficked to peroxisomes or that peroxisomes gathered to the Pex30p-GFP punctae.

To investigate the ER localization of Pex30p in more detail, we monitored the fluorescent signals in cells coexpressing Rtn1p-mCherry and Pex30p-GFP (Fig. 4*D*). As previously reported (51), Rtn1p-mCherry localized to ER tubules. Likewise, Pex30p-GFP localized throughout the ER, but both proteins accumulated in punctate structures predominantly located at the cell periphery as exemplified by the line profiles of chosen accumulations (Fig.4*D*).

Our microscopic analyses revealed that under conditions that promoted peroxisome proliferation, Pex30p localized primarily to subdomains of the cortical ER at boundaries between ER tubules and peroxisomes (Fig. 4*C* and 4*D*), whereas on glucose no drastic accumulation of Pex30p-GFP could be observed (Fig. 4*E*). In agreement with this observation, in early peroxisome proliferation (8 h), the Pex30p binding partners Pex29p and Pex32p also localized to the ER. However, at a later time point (16 h), although Pex29p was still mostly present in the ER, Pex30p accumulated in punctae with peroxisomes in close vicinity and Pex32p trafficked to peroxisomes (supplemental Fig. S5).

Reticulon Proteins Control Peroxisome Proliferation—The RHPs Rtn1p, Rtn2p and Yop1p are known to participate in the maintenance of the positive membrane curvature and tubulation and primarily partition to cortical ER tubules (46, 52). Because RHPs were found to specifically associate with Pex30p via SILAC-AP-MS experiments and a portion of Rtn1p colocalized with Pex30p-GFP, we assessed the effect of deleting Rtn1p on Pex30p localization. In these cells, another RHP, mCherry-tagged Yop1p, localized to tubular ER structures and accumulated in spots containing Pex30p-GFP (Fig. 5*A*). However, overproduction of Rtn1p altered the distribution of Pex30p-GFP and our data show that no Pex30p-GFP punctae could be seen in *rtn1*Δ cells expressing plasmid-borne Rtn1p.

To evaluate whether all three RHPs acted on peroxisome proliferation, we next analyzed the effect of deleting these three factors on peroxisome abundance (Fig. 5*B*). The *rtn1*Δ*rtn2*Δ*yop1*Δ mutant cells presented an atypical ER structure lacking the characteristic tubules (46) (Fig. 5*C*). These cells contained more peroxisomes than wild-type cells (11 ± 2.3 *versus* 7.8 ± 1.5; $n > 130$) and, strikingly, peroxisomes accumulated in small clusters of two to four peroxisomes similar to the effect observed in cells lacking Pex28p, Pex29p or both proteins (19). Furthermore, peroxisomes were

supernatants from fractions treated with TEV protease (Eluates) were analyzed by immunoblotting using anti-Pex30p antibodies. The levels of Rtn1$^{-\mathbf{TAP}}$ detected in the input fractions serve as loading control. In the last two lanes of the right panel, wild-type cells contained multicopy plasmids expressing *PEX29* either controlled by the *ADH1*- or the endogenous *PEX29*-promoter. *B*, Pex30p localizes to the ER. *pex30*Δ cells expressing plasmid-borne Sec63p-RFP (red channel) and Pex30p-GFP (green channel) controlled by the *GAL*-promoter were treated as described in Fig. 1. A region of interest was chosen to illustrate through line profiling that the large Pex30p-GFP accumulations (green punctae), although partially colocalizing, did not coincide with accumulations of Sec63p-RFP (see arrow, dashed lines, and profiles). The blue color depicts the cell wall obtained from transmission images. *C*, Peroxisomes accumulate near Pex30p-GFP punctae. Mutant *pex30*Δ cells expressing the peroxisomal marker protein mCherry-Px (red channel) and plasmid-borne Pex30p-GFP (green channel) were cultured as described in Fig. 1. Colocalization was analyzed for the indicated cells as depicted in the color-coded maps for spatial discrimination. A region of interest was chosen to illustrate through line profiling the high fluorescent signal of Pex30p-GFP accumulations (green punctae) in comparison with accumulations of mCherry-Px punctate signal. Correlation between peroxisomes and Pex30p is indicated (arrowheads). *D*, Pex30p-GFP colocalizes with Rtn1p-mCherry in the ER. Cells expressed Rtn1p-mCherry (red channel) from the *RTN1* genomic locus and plasmid-borne Pex30p-GFP (green channel). The perinuclear ER contained less Rtn1p-mCherry signal (arrow). Line profiles were established for chosen regions of the cortical ER in which both Rtn1p-mCherry and Pex30p-GFP accumulated in large punctate structures (arrowheads). *E*, In contrast, in cells grown on glucose-containing medium, Pex30p-GFP does not seem to accumulate in large punctate structures. On either growth conditions, the Rtn1p-mCherry stainings were indistinguishable (*D*, *E*).

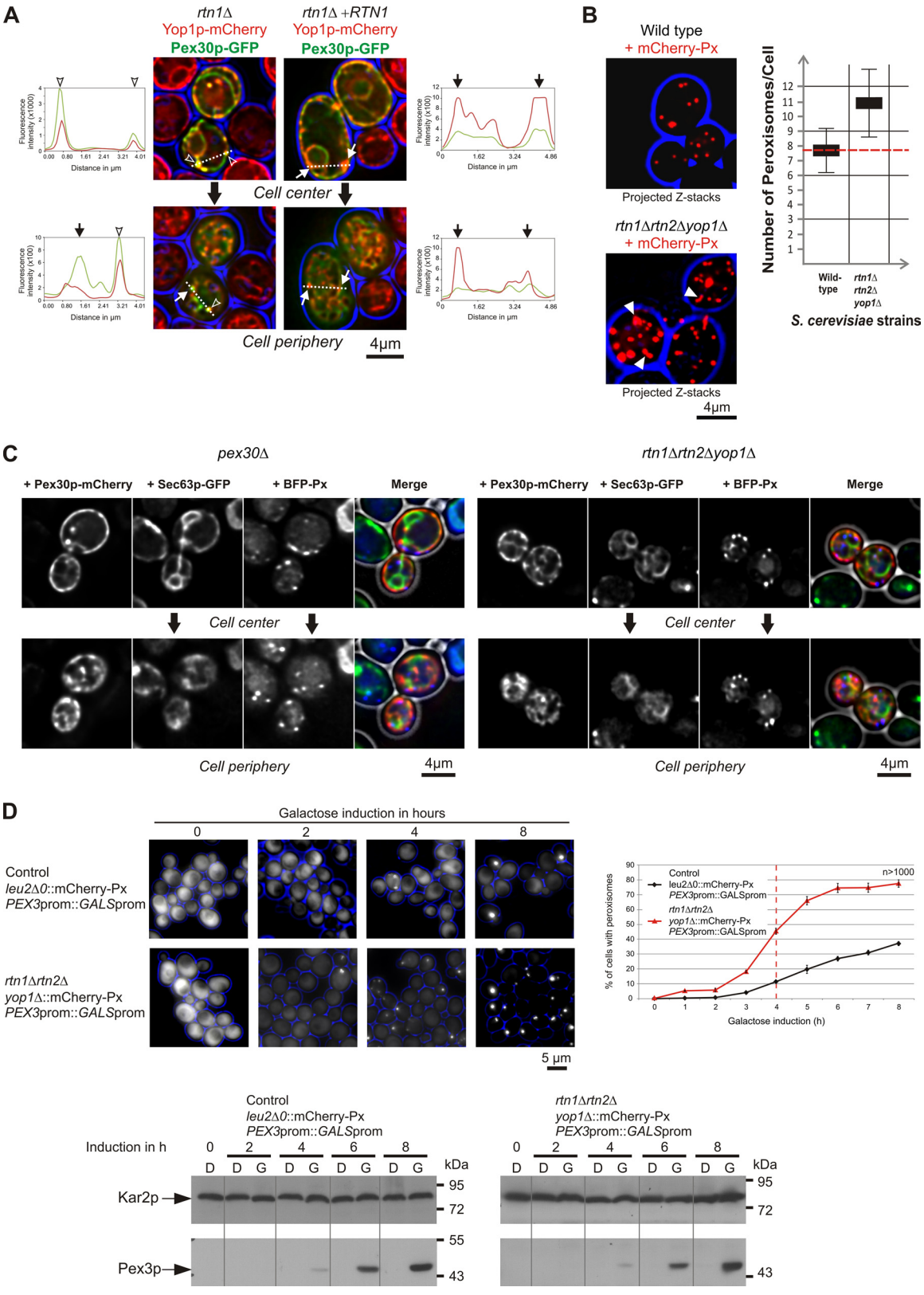

FIG. 5. **The cortical ER and reticulon homology proteins control *de novo* biogenesis of peroxisomes.** *A*, Overproduction of Rtn1p alters the distribution of Pex30p-GFP. Mutant cells *rtn1Δ* (left panel) and *rtn1Δ* with plasmid-encoded Rtn1p (right panel) expressing Yop1p-mCherry (red channel) from the *YOP1* genomic locus were transformed with plasmids coding for Pex30p-GFP (green channel). Cells were treated as

functional in cells lacking RHPs as evaluated by their ability to use oleic acid (data not shown).

RHPs Regulate the Efficiency of De Novo Peroxisome Biogenesis From the ER—To test whether RHPs were involved in peroxisome biogenesis, we established an *in vivo* biogenesis assay based on the transcriptional control of the essential peroxin *PEX3* through the *GAL*-promoter. Cells lacking Pex3p are devoid of peroxisomes and when Pex3p is reintroduced in these cells, peroxisomes are slowly generated *de novo* from the ER (7). We performed time lapse imaging of cells with (control) or without RHPs (*rtn1*Δ*rtn2*Δ*yop1*Δ) expressing *GAL*-driven *PEX3* during galactose induction and evaluated the time required to obtain mature peroxisomes revealed by fluorescent mCherry-Px dots. No peroxisome was present in cells cultured on glucose medium as illustrated by the presence of mCherry-Px in the cytosol (Fig. 5*D*, left panel). Strikingly, although control cells needed 3 to 4 h galactose induction to produce peroxisomes (mCherry-Px dots), in mutants lacking the RHPs cells containing peroxisomes were already observable 1 h after induction. After 4 h induction, the difference was even greater between the two strains (Fig. 5*D*, right panel). Moreover, similar to cells lacking RHPs only, peroxisomes accumulated in small clusters. These observations were not due to varying levels of Pex3p between both strains (Fig. 5*D*, bottom panel). Consequently, our data illustrate that *de novo* peroxisome biogenesis from the ER is enhanced in the absence of RHPs. This strongly suggests that the ER membrane architecture plays an essential role in the regulation of peroxisome maintenance in yeasts.

Pex30p Traffics From the Perinuclear Area to Punctae at the Cortical ER—We further tested whether Pex30p trafficked through the ER and measured fluorescence recovery after photobleaching (FRAP) on living yeast cells expressing either Sec63p-GFP or Pex30p-GFP. The Sec63p-GFP signal recovered within a few seconds after bleaching regardless of whether the perinuclear ER or the cortical ER had been bleached (Fig. 6*A*). For Pex30p-GFP, we bleached three different regions, namely, (1) the perinuclear area, (2) the cortical ER, and, (3) a punctate structure at the cell periphery. The first two areas showed partial recovery, whereas the fluorescent signal of the Pex30p-GFP punctae did not recover substantially. Instead, a tubular structure with fluorescence appeared at the bleached positions. These data demonstrate that Pex30p-GFP molecules are freely diffusible when present in the perinuclear region and in the cortical ER but fairly static in the punctate structures at the cell periphery. Considering that peroxisomes do not contain Rtn1p (12) and that the Pex30p punctae colocalized with Rtn1p (Fig. 4*D*), these most likely represent specific ER subdomains.

ER-to-Peroxisome Contact Sites Control Peroxisomal Dynamics—Peroxisomes (mCherry-Px) accumulated near the Pex30p-GFP signals (Fig. 4*C*). This observation suggested that a portion of the peroxisomal population might be in contact with the ER through interaction with Pex30p. To test this possibility, we analyzed living yeast cells grown under peroxisome proliferating conditions following a short galactose pulse to induce Pex30p-GFP expression and monitored the fate of fluorescent signals with time. Pex30p-GFP exhibited clear ER staining that rapidly accumulated into punctate structures. Moreover, peroxisomes (mCherry-Px) appeared to concentrate at Pex30p-GFP accumulation sites suggesting a molecular connection between peroxisomes and Pex30p at specific ER domains (Fig. 6*B*; Movie S1). Notably, shortly before cell division, Pex30p-GFP concentrated at the tip of the bud and peroxisomes were consistently present near these structures. Upon cell division, Pex30p-GFP molecules present at the bud tip diffused back into the cortical ER after cytokinesis (Movie S1).

We noticed that the peroxisomes present near the Pex30p-GFP punctae at the ER clearly lacked rapid movement. In contrast, free peroxisomes showed rapid motion. Thus, to be able to quantify the effect of Pex30p expression on peroxisome motility, we recorded peroxisome movements in *pex30*Δ cells with or without Pex30p-GFP. Peroxisomes in contact with Pex30p-GFP punctae remained associated for the entire time of the experiment (30 min), which clearly points to a stable connection between these two entities. The average center-to-center distance between ER-attached peroxi-

described in Fig. 1. The arrows point to the accumulation of both Yop1p-mCherry and Pex30p-GFP in punctate structures in cells lacking Rtn1p. Colocalization of these structures is illustrated through line profiling of a region of interest (arrowheads). In contrast, in cells overexpressing Rtn1p the Pex30p-GFP fluorescent signal was present throughout the ER without major accumulations as illustrated in the line profiles (arrows). Line scans illustrate that with or without Rtn1p the Yop1-mCherry stainings show accumulations. *B*, Cells lacking RHPs contain an elevated number of peroxisomes. Wild-type cells and cells lacking Rtn1p, Rtn2p and Yop1p were treated as described in Fig. 1 and images were acquired for mCherry-Px (red channel). Note the tendency of peroxisomes to cluster in the mutant cells (arrowheads). The average number of fluorescent mCherry-Px dots per cell is indicated as mean ± S.D. (right panel). The dashed red line represents the average number of peroxisomes in wild-type cells. *C*, Localization of Pex30p-mCherry with respect to Sec63p-GFP (ER) and BFP-Px (peroxisomes) in cells lacking Pex30p or the RHPs (as indicated). *D*, Peroxisome biogenesis in cells lacking RHPs. Peroxisome biogenesis was monitored through expression of *GAL*-driven *PEX3* in control cells or in cells lacking the RHPs chromosomally expressing mCherry-Px as indicated. The graph shows the percentage of cells containing peroxisomes in dependence of the incubation time in galactose medium. Protein extracts were analyzed by immunoblotting for the indicated time points (D, Dextrose; G, Galactose). Equal amounts of proteins were loaded in each lane. After protein transfer onto nitrocellulose, the membrane was cut in two parts; the upper part was probed with anti-Kar2p (Kar2p, 74.4 kDa) and the lower part with anti-Pex3p (Pex3p, 50.6 kDa) antibodies.

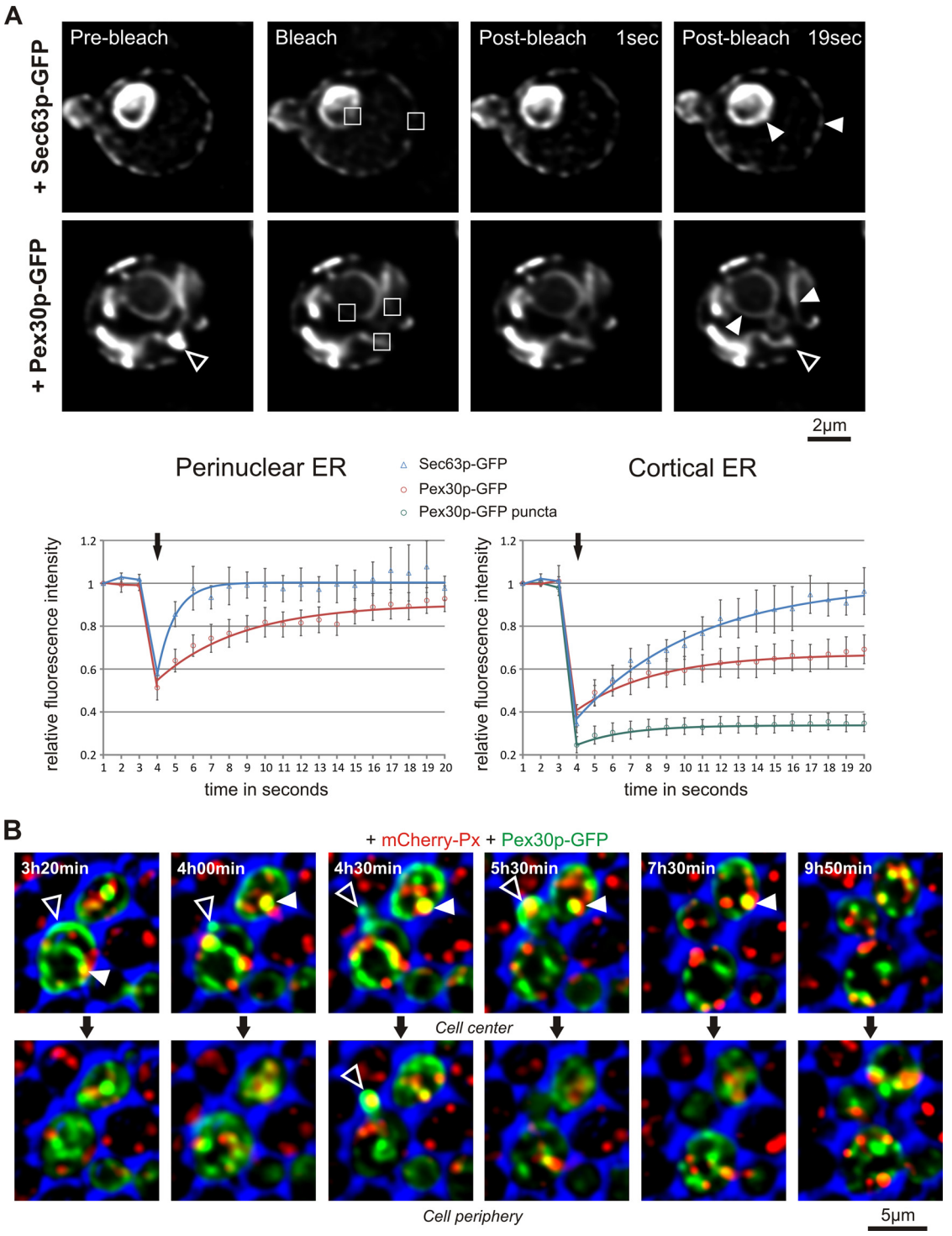

FIG. 6. **Pex30p traffics through the ER and peroxisomes adhere to Pex30p patches at ER subdomains.** *A*, FRAP experiments in *pex30*Δ yeast cells expressing either Sec63p-GFP or Pex30p-GFP (green channel). Small regions of the perinuclear or cortical ER fluorescence were bleached as indicated and fluorescence recovery was monitored (closed arrowhead, upper panel). For Pex30p-GFP, three regions were chosen for bleaching as indicated and fluorescence recovery was monitored within the perinuclear and the cortical ER (closed arrowheads) as well as in a fluorescent dot at the cell periphery (open arrowhead). The images show representative experiments. Quantifications of fluorescence intensities from at least five independent experiments are illustrated for each studied region. Error bars represent the standard error. *B*, Dynamics of Pex30p-GFP in growing cells. The fluorescence emitted by mCherry-Px (red channel) and Pex30p-GFP (green channel) was monitored live starting 3 h after plating the cells on agarose pads containing oleic acid. A portion of the mCherry-Px signal gathered to the Pex30p-GFP accumulations forming at later time points (closed arrowheads) and at the bud tip (open arrowhead).

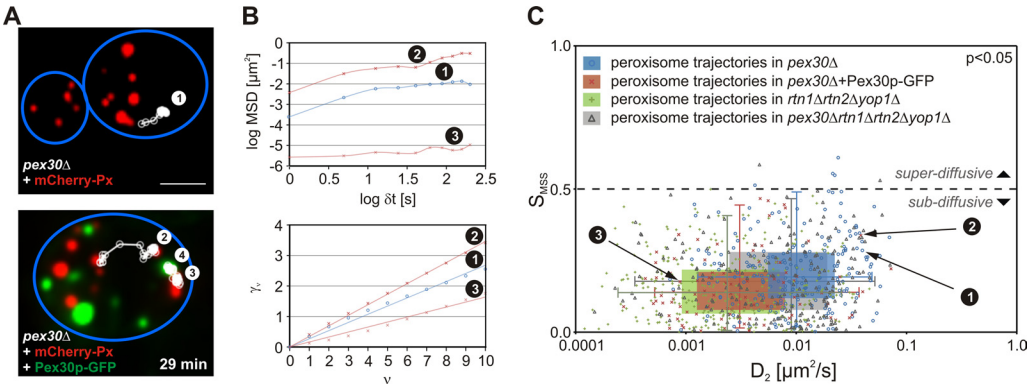

FIG. 7. **Peroxisome diffusion and targeted movement decrease in the absence of Pex30p.** *A*, Mutant *pex30*Δ cells expressing either mCherry-Px (red channel) only or plasmid-borne Pex30p-GFP (green channel) in addition were imaged in 60 s intervals. Representative trajectories of peroxisomes (mCherry-Px dots) are shown in a *pex30*Δ cell (#1) and in a *pex30*Δ cell expressing Pex30p-GFP (#2 and #3). Trajectory #2 corresponds to a mobile peroxisome, whereas trajectory #3 remained close to the depicted Pex30p-GFP puncta (#4). Cell walls are shown based on transmission images (blue color). *B*, Analysis of the peroxisomal trajectories (#1–3) shown in (*A*) for two different parameters: the mean square displacement (MSD, upper plot) allows for the calculation of the diffusion coefficients (D_2). The slopes of the corresponding moment scaling spectra (MSS, lower plot) help discriminating the type of motion. *C*, Scatter plot summarizing all peroxisomal trajectories studied. The plot shows the diffusion coefficients (D_2) extracted from the MSD diagram in function of the slope extracted from the MSS (S_{MSS}). The trajectories of all peroxisomes are indicated for *pex30*Δ mutant cells (blue circles; $n = 251$), *pex30*Δ expressing Pex30p-GFP (red crosses; $n = 108$), *rtn1*Δ*rtn2*Δ*yop1*Δ cells (green crosses; $n = 327$) and for *pex30*Δ*rtn1*Δ*rtn2*Δ*yop1*Δ (gray triangles; $n = 197$). For each strain studied, trajectories derived from measurements of all visible peroxisomes (mCherry-Px dots; n indicated) in more than 10 cells. For each peroxisomal population a two-dimensional box plot was overlaid and the statistical significance in both S_{MSS} and D_2 for cells with or without Pex30p (red and green *versus* blue and gray data) was assessed using a Wilcoxon rank sum test as indicated under "Experimental Procedures" ($p < 0.05$).

somes (mCherry-Px) and Pex30p-GFP punctae was smaller than 850 nm. In some cases, the structures even intersected confirming the association (Fig. 7*A*, Movie S2).

In the absence of Pex30p, we frequently observed an increase in peroxisomal movement. Thus, we sought to examine the trajectories of several peroxisomal populations. In *pex30*Δ cells, most peroxisomes were extremely mobile and exhibited a high percentage of directed trajectories, some of which even breaking the sub-diffusive regime. Accordingly, in *pex30*Δ cells expressing plasmid-borne Pex30p-GFP, peroxisomes displayed slower diffusion (low D_2) and less directed movement (low MSS slopes; Figs. 7*A*–7*C*). Similar observations were made when we compared the trajectories of peroxisomes in cells lacking the RHPs with those of peroxisomes in cells lacking Pex30p in addition. Considering that half of the peroxisomal population was present on Pex30p-GFP punctae (Fig. 6*B*, Movie S1), these data point to a direct role for Pex30p in the establishment of ER-to-peroxisome associations whereas RHPs may provide an architectural advantage by maintaining a highly curved ER membrane.

Pex30p Coordinates De Novo Peroxisome Biogenesis—Although peroxisomes can be formed *de novo* from the ER, studies in yeasts showed that under normal conditions, peroxisomes rather use the growth and division pathway to proliferate (53). *De novo* formation only occurs in mutant cells devoid of peroxisomes in which the missing gene is reintroduced. This is associated with the budding of pre-peroxisomal vesicles from specialized ER subdomains that represent peroxisome exit sites (54). These exit sites may possibly match the contact sites observed in wild-type cells. To test this hypothesis, we needed cells that could proceed to both *de novo* formation and growth or division of peroxisomes and established an assay based on the recent finding that in *S. cerevisiae* peroxisomes are actively inherited during cell division. Here, the antagonistic action of two proteins, Inp1p and Inp2p, controls inheritance of the peroxisomal population. Although Inp1p anchors peroxisomes to the cortex of the mother cell, Inp2p counters it by connecting peroxisomes to Myo2p, a myosin motor protein that transports peroxisomes in the daughter cell along actin cables (21). We used these findings and performed live-cell imaging to analyze peroxisomes in microcolonies growing from single cells lacking either Inp1p or Inp2p (Fig. 8 and supplemental Fig. S6). Fig. 8 illustrates that control cells contained peroxisomes (mCherry-Px dots) all through cell division, whereas after division *inp2*-mutant daughter cells lacked peroxisomes. However, these daughter cells slowly regained peroxisomes through *de novo* biogenesis leading to about 50% of cells with peroxisomes in the microcolonies (53). Interestingly, in the additional absence of Pex30p, more cells contained peroxisomes in the microcolonies (Fig. 8*B*, panel3). This was not because of a rescue of the inheritance defect as shown in the first division steps. Note that these cells also contained more peroxisomes than *inp2*Δ cells, showing that absence of Pex30p strongly affected *de novo* biogenesis of peroxisomes.

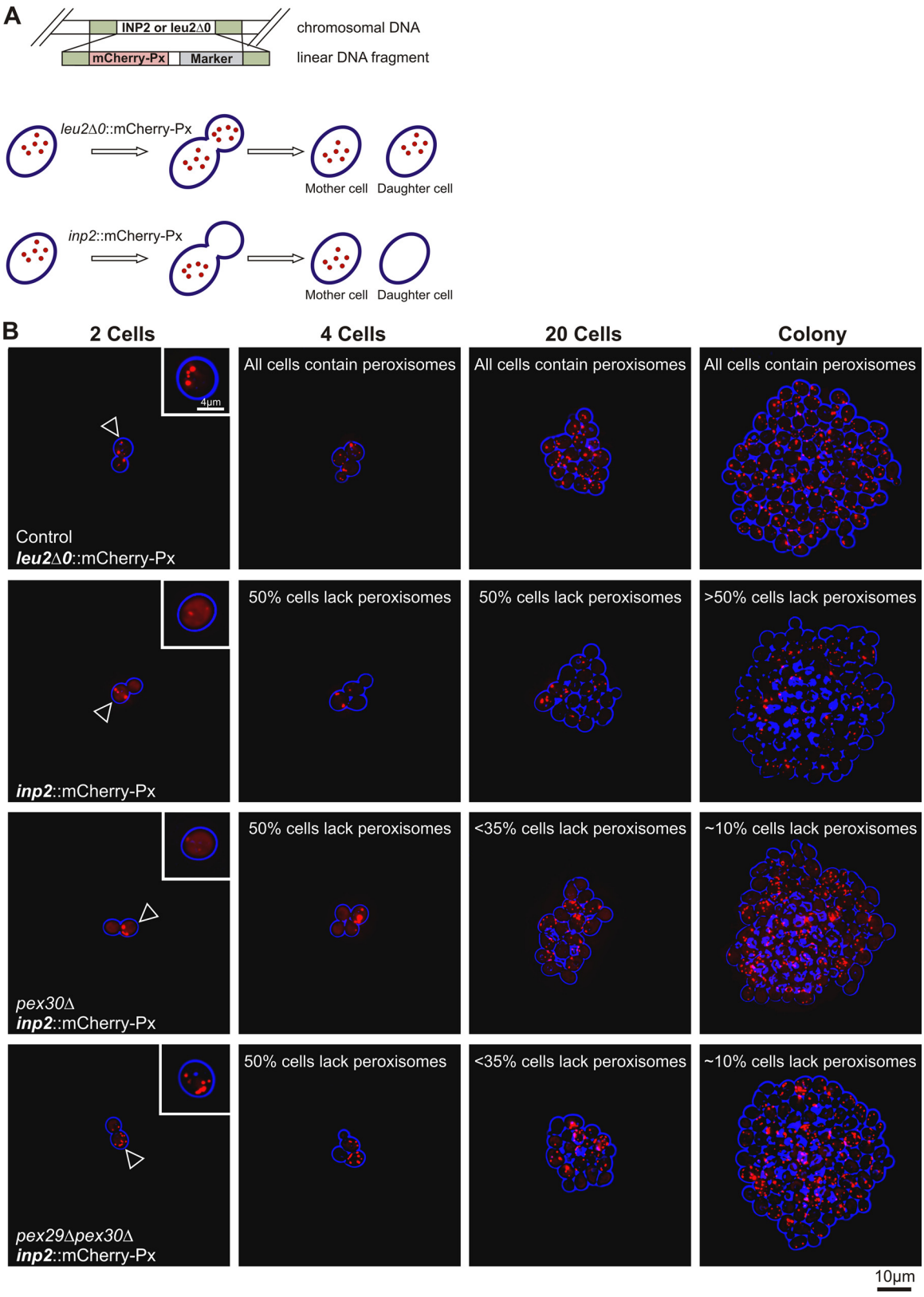

FIG. 8. **De novo biogenesis of peroxisomes is enhanced in cells lacking Pex30p.** *A*, Cartoon showing the retention of peroxisomes in the mother cell in mutants lacking Inp2p. In wild-type cells, the number of peroxisomes doubles shortly before cell division and both mother and daughter inherit half of the peroxisome pool. In the absence of Inp2p, all peroxisomes are retained in the mother cell upon cell division.

DISCUSSION

The work presented herein provides a thorough analysis of distinct membrane proteins acting in the regulation of peroxisome biogenesis in connection with the ER. Our findings expand the current insights into peroxisome proliferation by demonstrating for the first time that the control of the peroxisomal number per cell also relies on proteins residing in the ER and on the integrity of the cortical ER tubular architecture.

We studied ER-to-peroxisome associations and identified connections between the organelles via quantitative interaction proteomics and imaging analyses. The Pex30p core complex contains two groups of proteins: 1) proteins regulating peroxisome proliferation, and 2) ER resident proteins (Fig. 2). Although in the yeast *P. pastoris* Pex30p was reported to localize to both the ER and peroxisomes (20), Pex30p from *S. cerevisiae* was previously described as a peroxisomal membrane protein (18). Our data demonstrate that, similar to Pex30p in *P. pastoris*, *Sc*Pex30p is present at several locations (Figs. 4–6). This finding raises new questions with regard to Pex30p trafficking and function. Thus, it was particularly interesting to analyze whether this protein transits through the ER and whether this is associated with its function in peroxisome proliferation. We provide evidence that Pex30p molecules undergo rapid transport through the ER network and segregate to subdomains of the cortical ER tubules (Fig. 6*A*). Our analyses of peroxisome dynamics further show that Pex30p accumulates at specialized ER subdomains in which RHPs are also present (Figs. 4*D*, 5*A*) suggesting that these domains represent *E*R-to-*p*eroxisomes *con*tact *s*ites (EPCONS) (Figs. 6*B*, 7*A*–7*C*). Associations of peroxisomes with the ER could possibly enable the transfer of material between both compartments. A recent study in yeast suggested that non-vesicular phospholipid transfer occurs between peroxisomes and the ER (55).

The proteins RTN4a and DP1 as well as Rtn1p, Rtn2p and Yop1p affect the curvature of the ER membrane in mammalian and yeast cells, respectively (46, 50, 56). These integral membrane proteins bend the phospholipid bilayer through generation of a wedge in the outer leaflet explaining their partitioning into and stabilization of highly curved ER tubules (46, 57). Although deletion of Rtn1p and Rtn2p affects the ER morphology only under stress conditions, the additional absence of Yop1p results in a disrupted tubular ER under normal growth conditions (46). Besides, atlastin proteins (Sey1p in yeast) were shown to be involved in the fusion of ER tubules to generate an interconnected membrane network (58). These proteins are therefore essential to maintain the netlike structure of the cortical ER. The different architectures of the ER membrane restrict biological processes to specialized areas (59). Moreover, very recent observations illustrate that specialized areas of the cortical ER mark sites for the division of mitochondria (60). Likewise, our results suggest that RHPs are also involved in the regulation of peroxisome biogenesis (Fig. 5*D*).

Although peroxisomes are known to originate from the ER, no resident ER protein had previously been identified that regulated this process. The existence of EPCONS as proposed here supports previous observations of ER subdomains that extend to peroxisomes (54). Thus EPCONS could represent a molecular platform required for the formation of peroxisomes. The tubular architecture of the cortical ER achieved through RHPs seems to be essential to regulate this process.

Our biochemical studies also substantiate a role for vesicular trafficking in the transport of distinct peroxisomal membrane proteins. Indeed, we identified all subunits of the COPI coatomer complex as transiently interacting partners of Pex30p suggesting a role in the retrograde transport of Pex30p (Figs. 2*B*, 3*A*–3*C*, supplemental Figs. S3, S4). Alternatively, the transport of Pex30p en route to peroxisomes may occur through formation of vesicular membrane clusters originating from the cortical ER, an event that may require the function of COPI vesicles. It has been shown that the early peroxin Pex3p accumulated to tubular-vesicular membrane structures in cells with hampered expression of COPI-vesicles tethering factors suggesting the involvement of the coatomer in peroxisome biogenesis (12). In agreement, ADP-ribosylation factors (Arfs), inherent components of the coatomer, were reported to bind peroxisomes *in vitro* (61). In *S. cerevisiae*, Arf1p was shown to be essential for the division of peroxisomes from existing peroxisomes and Arf3p stimulated proliferation (62). Interestingly, Pex30p is the only peroxin in the yeast *S. cerevisiae* whose amino acid sequence ends with an ER-retrieval dilysine motif (-KKXX) (see also 63). The presence of this motif suggests a mechanism to ensure the presence of Pex30p proteins in the ER membrane.

Morphological data published in the 1970s already showed the proximity of peroxisomes and the ER in mammalian cells (64) but whether both organelles effectively connect and how the organellar interface is established is not known. It is tempting to speculate that EPCONS do not only provide a connecting platform for pre-existing peroxisomes for growth/division but also represent ER exit sites during *de novo* biogenesis allowing for tight coordination of these two processes.

Peroxisomes are slowly regenerated *de novo* in daughter cells. *B*, Peroxisomal biogenesis assay in inheritance mutant cells. Cells expressing mCherry-Px were plated onto agarose pads containing glucose medium and the formation of microcolonies originating from single cells were observed live for a total of 12 h in 15 min intervals. The experiments were performed on three independent cultures. Each time, eight single cells were imaged simultaneously, one example of which is shown for each strain as indicated. Note that cells lacking Pex30p or Pex29p and Pex30p contain many peroxisomes. The arrowheads indicate mother cells.

Acknowledgments—We thank Jeffrey Gerst for comments and suggestions on drafts of the manuscript. We thank Andreas Hartig for the plasmid coding for yeast Pex3p and for expert support, Alexander Wöran for his excellent technical assistance as well as Klaus Jung for discussion.

* This work was supported by grants from the Austrian Science Fund (FWF) P-20803 to CB and from the Deutsche Forschungsgemeinschaft (FOR1905) to BW and RE, and the Excellence Initiative of the German Federal & State Governments (EXC 294 BIOSS Centre for Biological Signalling Studies) to BW. CB was supported by the Elise-Richter-Program (V39-B09) of the Austrian Science Fund (FWF) and the Austrian Federal Ministry for Science and Research (BMWF).

S This article contains supplemental Tables S1 to S5, Figs. S1 to S6 and Movies S1 and S2.

‖ To whom correspondence should be addressed: Cécile Brocard, Tissue Med Biosciences Forschungs- und Entwicklungsgesellschaft mbH, Magnesitstrasse 1, A-3500 Krems, Austria. Tel.: +43/2732/87470-300; Fax: +43/2732/87470-4061; E-mail: cecile.brocard@univie.ac.at; cb@tmbiosciences.com; or Bettina Warscheid, Tel.: +49 761 203 2690, Fax: +49 761 203 2601, E-mail: bettina.warscheid@biologie.uni-freiburg.de.

** The authors contributed equally to this work.

REFERENCES

1. Wanders, R. J., and Waterham, H. R. (2006) Biochemistry of mammalian peroxisomes revisited. *Annu. Rev. Biochem.* **75,** 295–332
2. Faust, P. L., Kaye, E. M., and Powers, J. M. (2010) Myelin lesions associated with lysosomal and peroxisomal disorders. *Expert Rev. Neurother.* **10,** 1449–1466
3. Fan, J., Quan, S., Orth, T., Awai, C., Chory, J., and Hu, J. (2005) The Arabidopsis PEX12 gene is required for peroxisome biogenesis and is essential for development. *Plant Physiol.* **139,** 231–239
4. Steinberg, S. J., Dodt, G., Raymond, G. V., Braverman, N. E., Moser, A. B., and Moser, H. W. (2006) Peroxisome biogenesis disorders. *Biochim. Biophys. Acta* **1763,** 1733–1748
5. Distel, B., Erdmann, R., Gould, S. J., Blobel, G., Crane, D. I., Cregg, J. M., Dodt, G., Fujiki, Y., Goodman, J. M., Just, W. W., Kiel, J. A., Kunau, W. H., Lazarow, P. B., Mannaerts, G. P., Moser, H. W., Osumi, T., Rachubinski, R. A., Roscher, A., Subramani, S., Tabak, H. F., Tsukamoto, T., Valle, D., van der Klei, I., van Veldhoven, P. P., and Veenhuis, M. (1996) A unified nomenclature for peroxisome biogenesis factors. *J. Cell Biol.* **135,** 1–3
6. Koch, J., and Brocard, C. (2011) Membrane elongation factors in organelle maintenance: the case of peroxisome proliferation. *Biomol. Concepts* **2,** 353–364
7. Hoepfner, D., Schildknegt, D., Braakman, I., Philippsen, P., and Tabak, H. F. (2005) Contribution of the endoplasmic reticulum to peroxisome formation. *Cell* **122,** 85–95
8. Toro, A. A., Araya, C. A., Córdova, G. J., Arredondo, C. A., Cárdenas, H. G., Moreno, R. E., Venegas, A., Koenig, C. S., Cancino, J., Gonzalez, A., and Santos, M. J. (2009) Pex3p-dependent peroxisomal biogenesis initiates in the endoplasmic reticulum of human fibroblasts. *J. Cell. Biochem.* **107,** 1083–1096
9. Kim, P. K., Mullen, R. T., Schumann, U., and Lippincott-Schwartz, J. (2006) The origin and maintenance of mammalian peroxisomes involves a de novo PEX16-dependent pathway from the ER. *J. Cell Biol.* **173,** 521–532
10. van der Zand, A., Braakman, I., and Tabak, H. F. (2010) Peroxisomal membrane proteins insert into the endoplasmic reticulum. *Mol. Biol. Cell* **21,** 2057–2065
11. Lam, S. K., Yoda, N., and Schekman, R. (2010) A vesicle carrier that mediates peroxisome protein traffic from the endoplasmic reticulum. *Proc. Natl. Acad. Sci. U.S.A.* **107,** 21523–21528
12. Perry, R. J., Mast, F. D., and Rachubinski, R. A. (2009) Endoplasmic reticulum-associated secretory proteins Sec20p, Sec39p, and Dsl1p are involved in peroxisome biogenesis. *Eukaryot. Cell* **8,** 830–843
13. Fagarasanu, A., Fagarasanu, M., Eitzen, G. A., Aitchison, J. D., and Rachubinski, R. A. (2006) The peroxisomal membrane protein Inp2p is the peroxisome-specific receptor for the myosin V motor Myo2p of Saccharomyces cerevisiae. *Dev. Cell* **10,** 587–600
14. Fagarasanu, M., Fagarasanu, A., Tam, Y. Y., Aitchison, J. D., and Rachubinski, R. A. (2005) Inp1p is a peroxisomal membrane protein required for peroxisome inheritance in Saccharomyces cerevisiae. *J. Cell Biol.* **169,** 765–775
15. Hoepfner, D., van den Berg, M., Philippsen, P., Tabak, H. F., and Hettema, E. H. (2001) A role for Vps1p, actin, and the Myo2p motor in peroxisome abundance and inheritance in Saccharomyces cerevisiae. *J. Cell Biol.* **155,** 979–990
16. Brown, T. W., Titorenko, V. I., and Rachubinski, R. A. (2000) Mutants of the Yarrowia lipolytica PEX23 gene encoding an integral peroxisomal membrane peroxin mislocalize matrix proteins and accumulate vesicles containing peroxisomal matrix and membrane proteins. *Mol. Biol. Cell* **11,** 141–152
17. Tam, Y. Y., and Rachubinski, R. A. (2002) Yarrowia lipolytica cells mutant for the PEX24 gene encoding a peroxisomal membrane peroxin mislocalize peroxisomal proteins and accumulate membrane structures containing both peroxisomal matrix and membrane proteins. *Mol. Biol. Cell* **13,** 2681–2691
18. Vizeacoumar, F. J., Torres-Guzman, J. C., Bouard, D., Aitchison, J. D., and Rachubinski, R. A. (2004) Pex30p, Pex31p, and Pex32p form a family of peroxisomal integral membrane proteins regulating peroxisome size and number in Saccharomyces cerevisiae. *Mol. Biol. Cell* **15,** 665–677
19. Vizeacoumar, F. J., Torres-Guzman, J. C., Tam, Y. Y., Aitchison, J. D., and Rachubinski, R. A. (2003) YHR150w and YDR479c encode peroxisomal integral membrane proteins involved in the regulation of peroxisome number, size, and distribution in Saccharomyces cerevisiae. *J. Cell Biol.* **161,** 321–332
20. Yan, M., Rachubinski, D. A., Joshi, S., Rachubinski, R. A., and Subramani, S. (2008) Dysferlin Domain-containing Proteins, Pex30p and Pex31p, Localized to Two Compartments, Control the Number and Size of Oleate-induced Peroxisomes in Pichia pastoris. *Mol. Biol. Cell* **19,** 885–898
21. Fagarasanu, A., Fagarasanu, M., and Rachubinski, R. A. (2007) Maintaining peroxisome populations: a story of division and inheritance. *Annu. Rev. Cell Dev. Biol.* **23,** 321–344
22. Manjithaya, R., Nazarko, T. Y., Farré, J. C., and Subramani, S. (2010) Molecular mechanism and physiological role of pexophagy. *FEBS Lett.* **584,** 1367–1373
23. Mann, M. (2006) Functional and quantitative proteomics using SILAC. *Nat. Rev. Mol. Cell Biol.* **7,** 952–958
24. Ong, S. E., Blagoev, B., Kratchmarova, I., Kristensen, D. B., Steen, H., Pandey, A., and Mann, M. (2002) Stable isotope labeling by amino acids in cell culture, SILAC, as a simple and accurate approach to expression proteomics. *Mol. Cell. Proteomics* **1,** 376–386
25. Hanahan, D. (1983) Studies on transformation of Escherichia coli with plasmids. *J. Mol. Biol.* **166,** 557–580
26. Huber, A., Koch, J., Kragler, F., Brocard, C., and Hartig, A. (2012) A subtle interplay between three pex11 proteins shapes de novo formation and fission of peroxisomes. *Traffic* **13,** 157–167
27. Koch, J., Pranjic, K., Huber, A., Ellinger, A., Hartig, A., Kragler, F., and Brocard, C. (2010) PEX11 family members are membrane elongation factors that coordinate peroxisome proliferation and maintenance. *J. Cell Sci.* **123,** 3389–3400
28. Brocard, C., Lametschwandtner, G., Koudelka, R., and Hartig, A. (1997) Pex14p is a member of the protein linkage map of Pex5p. *EMBO J.* **16,** 5491–5500
29. Sandmann, T., Herrmann, J. M., Dengjel, J., Schwarz, H., and Spang, A. (2003) Suppression of coatomer mutants by a new protein family with COPI and COPII binding motifs in Saccharomyces cerevisiae. *Mol. Biol. Cell* **14,** 3097–3113
30. Höhfeld, J., Veenhuis, M., and Kunau, W. H. (1991) PAS3, a Saccharomyces cerevisiae gene encoding a peroxisomal integral membrane protein essential for peroxisome biogenesis. *J. Cell Biol.* **114,** 1167–1178
31. Albertini, M., Rehling, P., Erdmann, R., Girzalsky, W., Kiel, J. A., Veenhuis, M., and Kunau, W. H. (1997) Pex14p, a peroxisomal membrane protein binding both receptors of the two PTS-dependent import pathways. *Cell* **89,** 83–92
32. Oeljeklaus, S., Reinartz, B. S., Wolf, J., Wiese, S., Tonillo, J., Podwojski, K., Kuhlmann, K., Stephan, C., Meyer, H. E., Schliebs, W., Brocard, C., Erdmann, R., and Warscheid, B. (2012) Identification of core components

and transient interactors of the peroxisomal importomer by dual-track stable isotope labeling with amino acids in cell culture analysis. *J. Proteome Res.* **11,** 2567–2580
33. Agne, B., Meindl, N. M., Niederhoff, K., Einwächter, H., Rehling, P., Sickmann, A., Meyer, H. E., Girzalsky, W., and Kunau, W. H. (2003) Pex8p: an intraperoxisomal organizer of the peroxisomal import machinery. *Mol. Cell* **11,** 635–646
34. Kaller, M., Liffers, S. T., Oeljeklaus, S., Kuhlmann, K., Röh, S., Hoffmann, R., Warscheid, B., and Hermeking, H. (2011) Genome-wide characterization of miR-34a induced changes in protein and mRNA expression by a combined pulsed SILAC and microarray analysis. *Mol Cell Proteomics* **10**, M111. 010462
35. Cox, J., and Mann, M. (2008) MaxQuant enables high peptide identification rates, individualized p.p.b.-range mass accuracies and proteome-wide protein quantification. *Nat. Biotechnol.* **26,** 1367–1372
36. Wiese, S., Gronemeyer, T., Ofman, R., Kunze, M., Grou, C. P., Almeida, J. A., Eisenacher, M., Stephan, C., Hayen, H., Schollenberger, L., Korosec, T., Waterham, H. R., Schliebs, W., Erdmann, R., Berger, J., Meyer, H. E., Just, W., Azevedo, J. E., Wanders, R. J., and Warscheid, B. (2007) Proteomics characterization of mouse kidney peroxisomes by tandem mass spectrometry and protein correlation profiling. *Mol. Cell. Proteomics* **6,** 2045–2057
37. Perkins, D. N., Pappin, D. J., Creasy, D. M., and Cottrell, J. S. (1999) Probability-based protein identification by searching sequence databases using mass spectrometry data. *Electrophoresis* **20,** 3551–3567
38. Pan, C., Olsen, J. V., Daub, H., and Mann, M. (2009) Global effects of kinase inhibitors on signaling networks revealed by quantitative phosphoproteomics. *Mol. Cell. Proteomics* **8,** 2796–2808
39. Sbalzarini, I. F., and Koumoutsakos, P. (2005) Feature point tracking and trajectory analysis for video imaging in cell biology. *J. Struct. Biol.* **151,** 182–195
40. Jaskolski, F., Mulle, C., and Manzoni, O. J. (2005) An automated method to quantify and visualize colocalized fluorescent signals. *J. Neurosci. Methods* **146,** 42–49
41. Erdmann, R., and Blobel, G. (1995) Giant peroxisomes in oleic acid-induced Saccharomyces cerevisiae lacking the peroxisomal membrane protein Pmp27p. *J. Cell Biol.* **128,** 509–523
42. Rottensteiner, H., Stein, K., Sonnenhol, E., and Erdmann, R. (2003) Conserved function of pex11p and the novel pex25p and pex27p in peroxisome biogenesis. *Mol. Biol. Cell* **14,** 4316–4328
43. Oeljeklaus, S., Meyer, H. E., and Warscheid, B. (2009) New dimensions in the study of protein complexes using quantitative mass spectrometry. *FEBS Lett.* **583,** 1674–1683
44. Hubner, N. C., Bird, A. W., Cox, J., Splettstoesser, B., Bandilla, P., Poser, I., Hyman, A., and Mann, M. (2010) Quantitative proteomics combined with BAC TransgeneOmics reveals in vivo protein interactions. *J. Cell Biol.* **189,** 739–754
45. Vermeulen, M., Eberl, H. C., Matarese, F., Marks, H., Denissov, S., Butter, F., Lee, K. K., Olsen, J. V., Hyman, A. A., Stunnenberg, H. G., and Mann, M. (2010) Quantitative interaction proteomics and genome-wide profiling of epigenetic histone marks and their readers. *Cell* **142,** 967–980
46. Voeltz, G. K., Prinz, W. A., Shibata, Y., Rist, J. M., and Rapoport, T. A. (2006) A class of membrane proteins shaping the tubular endoplasmic reticulum. *Cell* **124,** 573–586
47. Prinz, W. A., Grzyb, L., Veenhuis, M., Kahana, J. A., Silver, P. A., and Rapoport, T. A. (2000) Mutants affecting the structure of the cortical endoplasmic reticulum in Saccharomyces cerevisiae. *J. Cell Biol.* **150,** 461–474
48. Wang, X., and Huang, L. (2008) Identifying dynamic interactors of protein complexes by quantitative mass spectrometry. *Mol. Cell. Proteomics* **7,** 46–57
49. Mousson, F., Kolkman, A., Pijnappel, W. W., Timmers, H. T., and Heck, A. J. (2008) Quantitative proteomics reveals regulation of dynamic components within TATA-binding protein (TBP) transcription complexes. *Mol .Cell. Proteomics* **7,** 845–852
50. Hu, J., Shibata, Y., Zhu, P. P., Voss, C., Rismanchi, N., Prinz, W. A., Rapoport, T. A., and Blackstone, C. (2009) A class of dynamin-like GTPases involved in the generation of the tubular ER network. *Cell* **138,** 549–561
51. Lee, S. C., Wu, C. H., and Wang, C. W. (2010) Traffic of a viral movement protein complex to the highly curved tubules of the cortical endoplasmic reticulum. *Traffic* **11,** 912–930
52. De Craene, J. O., Coleman, J., Estrada de Martin, P., Pypaert, M., Anderson, S., Yates, J. R., 3rd, Ferro-Novick, S., and Novick, P. (2006) Rtn1p is involved in structuring the cortical endoplasmic reticulum. *Mol. Biol. Cell* **17,** 3009–3020
53. Motley, A. M., and Hettema, E. H. (2007) Yeast peroxisomes multiply by growth and division. *J. Cell Biol.* **178,** 399–410
54. Geuze, H. J., Murk, J. L., Stroobants, A. K., Griffith, J. M., Kleijmeer, M. J., Koster, A. J., Verkleij, A. J., Distel, B., and Tabak, H. F. (2003) Involvement of the endoplasmic reticulum in peroxisome formation. *Mol. Biol. Cell* **14,** 2900–2907
55. Raychaudhuri, S., and Prinz, W. A. (2008) Nonvesicular phospholipid transfer between peroxisomes and the endoplasmic reticulum. *Proc. Natl. Acad. Sci. U.S.A.* **105,** 15785–15790
56. Shibata, Y., Hu, J., Kozlov, M. M., and Rapoport, T. A. (2009) Mechanisms shaping the membranes of cellular organelles. *Annu. Rev. Cell Dev. Biol.* **25,** 329–354
57. Zurek, N., Sparks, L., and Voeltz, G. (2011) Reticulon short hairpin transmembrane domains are used to shape ER tubules. *Traffic* **12,** 28–41
58. Rismanchi, N., Soderblom, C., Stadler, J., Zhu, P. P., and Blackstone, C. (2008) Atlastin GTPases are required for Golgi apparatus and ER morphogenesis. *Hum. Mol. Genet.* **17,** 1591–1604
59. Lynes, E. M., and Simmen, T. (2011) Urban planning of the endoplasmic reticulum (ER): how diverse mechanisms segregate the many functions of the ER. *Biochim. Biophys. Acta* **1813,** 1893–1905
60. Friedman, J. R., Lackner, L. L., West, M., DiBenedetto, J. R., Nunnari, J., and Voeltz, G. K. (2011) ER tubules mark sites of mitochondrial division. *Science* **334,** 358–362
61. Passreiter, M., Anton, M., Lay, D., Frank, R., Harter, C., Wieland, F. T., Gorgas, K., and Just, W. W. (1998) Peroxisome biogenesis: involvement of ARF and coatomer. *J. Cell Biol.* **141,** 373–383
62. Lay, D., Grosshans, B. L., Heid, H., Gorgas, K., and Just, W. W. (2005) Binding and functions of ADP-ribosylation factor on mammalian and yeast peroxisomes. *J. Biol. Chem.* **280,** 34489–34499
63. Cosson, P., and Letourneur, F. (1994) Coatomer interaction with di-lysine endoplasmic reticulum retention motifs. *Science* **263,** 1629–1631
64. Novikoff, A. B., Novikoff, P. M., Ma, M., Shin, W. Y., and Quintana, N. (1974) Cytochemical studies of secretory and other granules associated with the endoplasmic reticulum in rat thyroid epithelial cells. *Adv. Cytopharmacol.* **2,** 349–368